

Chapter 6

Positron scattering from molecules of biological interest

In the present chapter we introduce and discuss positron scattering cross sections for six targets that are important from a biological perspective: formic acid, tetrahydrofuran, 3-hydroxy-tetrahydrofuran, tetrahydrofurfuryl alcohol, 3,4-dihydropyran and pyrimidine. Except for tetrahydrofuran, the TCSs presented in this chapter have been individually published in Zecca *et al.* (2008a; 2008c; 2009a; 2010c; 2011a) and some of them have also been collectively reviewed in the papers by Brunger *et al.* (2009) and Chiari *et al.* (2012).

6.1 Introduction

Research on cross section measurements for lepton collisions with atoms and molecules has recently obtained some renewed interest within the scientific community (Brunger *et al.*, 2009). As anticipated in the previous chapter, this is mainly due to the fact that the study of lepton scattering from biomolecules has become of particular relevance in the field of atomic and molecular physics (ATMOP) and the medical science community since the early 2000's. The ultimate aim of this program is investigating the potential effects that high and low energy charged particles may cause when entering the human body, specifically during standard medical therapies or conventional diagnostic tests.

A thorough explanation of the reason for inspecting specifically positron scattering from biomolecules is given by Surdutovich *et al.* (2008), so here we provide only the main motivations that ultimately rationalise the work presented in this chapter. We also limit our discussion here to the case of positron collisions only. We first note that there are still many unanswered questions about the interactions of positrons with biomolecules, in particular concerning radiation damage on biomolecular systems (Brunger and Zecca, 2009). The seminal paper by Boudaiffa *et al.* (2000), in particular, questioned whether ballistic impacts were responsible for the majority of cell and tissue damage when ionising radiation, such as positrons used in positron emission tomography (PET), enters the human body. PET is a non-

invasive, medical imaging technique now widely used to produce three-dimensional representations of the functional processes taking place in the body. The main application of PET scans is as an early detection tool for tumours and as a general diagnostic device of metabolic activity. This kind of test requires a positron-emitting radionuclide, called a tracer, to be introduced into the body on a biologically active molecule. PET scans involve the detection of gamma rays pairs emitted by the annihilation events arising between the high-energy positrons emitted by the tracer and the electrons. The processes occurring between the emission of the high-energy particle and the gamma ray production obviously involve positron-molecule interactions.

Most medical devices initially start with very high-energy ionising radiation entering the human body, whether that be charged particles (positrons, electrons or heavy ions), like in PET, or photons (e.g. X-rays). It is actually now well understood and widely accepted that the major part of the energy deposited in soft matter by the initial high-energy radiation quickly thermalises in the body through processes such as direct ionisation, which, in turn, leads to the liberation of significant numbers of secondary electrons with typical energies ultimately below ~ 20 eV (Michael and Neil, 2000; Levesque *et al.*, 2005; Makochekanwa *et al.*, 2009). These secondary electrons continue to thermalise as they travel through the body until at lower energies, even well below the ionisation thresholds (Boudaiffa *et al.*, 2000) and discrete excitation (Martin *et al.*, 2004) thresholds, they may subsequently attach to or cause the fragmentation of DNA, proteins, and their various components (i.e. the nucleobases, sugars and water) (Boudaiffa *et al.*, 2000). Through the process of dissociative electron attachment these events may induce significant single- and double-strand breaks in DNA or the formation of free radicals, which through chemical reactions with DNA can also cause strand breaking (Boudaiffa *et al.*, 2000; Hassan *et al.*, 2000). All these processes can eventually result in important cell and tissue damage (Abdoul-Carime *et al.*, 2004; Levesque *et al.*, 2005).

We stress here that the mechanisms leading to biological damage are qualitatively and quantitatively different for positrons and electrons. In fact, the fundamental interactions driving the low-energy lepton-molecule scattering process, the static and dipole interactions, are quite different for positrons and electrons. As already noted previously, the static interaction is attractive for electrons and repulsive for positrons, while the polarization potential is negative in both cases. As a result, the magnitude of the positron and electron TCSs (see e.g. Zecca *et al.*, 2005 and next paragraphs) is different below a few tens of eV, with the TCS for positrons being expected to be lower in magnitude than their corresponding TCS for electrons. This discrepancy reflects also the presence of the exchange scattering channel in low energy collisions involving electrons, whereas this physical process does not occur with positrons. However, this is somewhat offset by the existence of positronium formation in the positron case, with both exchange and positronium formation becoming negligible above 100-300 eV projectile energies, so that the TCSs tend to merge in magnitude. The presence of the positronium formation channel in positron impact

phenomena on biomolecular systems potentially makes an even larger difference compared to electron scattering events, because of the ionising effect of the gamma ray photons resulting from positronium annihilation, which add to the gamma rays emitted by the annihilation of the positrons inside the organic tissue.

Application of positrons to research in the medical science field has recently expanded to beyond diagnosis techniques. Currently, there is a growing interest in utilising positrons in a therapeutic or clinical sense: as probes for protein syneresis (van Vliet *et al.*, 1991), for bioactive molecule encapsulation (Bögerhausen *et al.*, 2005) and even treatment of tumours (positherapy) (Menichetti *et al.*, 2009). Studying the interaction between positrons and biomolecules and understanding radiation dose rates is thus essential in applying those techniques. Nevertheless, there is essentially no fundamental, quantitative knowledge of these interactions yet. Current methods are still often based on models assuming that positrons behave almost like electrons, thus missing the real physics in the interaction processes, as represented by the scattering cross sections. As a consequence, positron scattering investigations from important biological compounds, e.g. the biomolecules that the nucleic acids DNA and RNA are made of, namely proteins, the nucleobases, sugars and also water, have become of topical interest in the scientific community.

It is worth noting that current developments in the biomedical applications of radiation, are necessitating increasingly higher levels of detail to understand the collisional processes leading to radiation damage in biological matter. In particular, therapies such as brachytherapy, where the radiation source is placed inside or close to the area needed to be treated, require an accurate calculation of the absorbed dose in matter and tissues in order to prescribe the treatment (Fuss *et al.*, 2010). In addition, an estimation of possible side effects in the surrounding areas, that may be particularly sensitive to ionising radiation, is also required. The description of radiation effects at the molecular level has fostered the need for quantifying radiation damage in nanovolumes, that is nanodosimetry. Nonetheless, rather than a simple measure of the energy deposited in the biological medium, which is probably not the best manner of illustrating the effects at the nanoscale, a detailed description of the interactions occurring in a nanosized target and their effect in terms of radiation damage is what is actually required. As this nanoregion of interest could be relatively far (approximately microns to even millimetres) from the original track of the incident high-energy primary particles, an accurate description of the single tracks of the secondary particles will be essential for that purpose.

Therefore, in addition to experimental scattering studies, the concurrent development of low-energy particle track simulation (LEPTS) codes, specifically intended to provide interaction details at the nanoscale, have lately become of relevant interest as well. There are now quite a few groups (see e.g. Fuss *et al.*, 2010; Muñoz *et al.*, 2008; Plante and Cucinotta, 2009; White and Robson, 2009 and references therein) using step-by-step Monte Carlo simulation techniques to reproduce the tracks of particles while moving through matter. Established examples of such models are

PENELOPE (Baro *et al.*, 1995) and GEANT4 (Agostinelli *et al.*, 2003; Allison *et al.*, 2006), while the low-energy particle track simulation code of the Madrid group (Muñoz *et al.*, 2008) appears to be the most recent. Such models ultimately aim at providing a nanoscale description of radiation damage in matter, but, in order to do so, they require a significant data base for the relevant atomic and molecular processes that occur in the biological matter. In the LEPTS code of the Madrid group (Muñoz *et al.*, 2008), for instance, accurate gas-phase spectroscopic data, absolute experimental and theoretical electron and positron scattering cross sections and energy loss distribution functions are employed as input parameters, in order to give a physical description of the particle tracks as they move through the medium in question. Simulating the effect of the interaction of radiation with matter, thus, requires a knowledge of the measured or calculated scattering cross sections (Muñoz *et al.*, 2008) for all the possible scattering processes. In particular TCSs, which are essentially the probability that some kind of collision will happen, are needed by scientists seeking to simulate the tracks of charged particles as they move through matter (Fuss *et al.*, 2010; Muñoz *et al.*, 2008) and are required to study the behaviour of positron swarm transport in various gases (Šuvakov *et al.*, 2008; Marler *et al.*, 2009). In the former case, TCSs are important as they specify the mean free path between collisions in such simulation studies. Note that in any modelling of PET, both positron and electron TCSs are required, as the fate of the incident high-energy positrons is to liberate many secondary lower-energy electrons, as a result of ionisation processes.

Further note also that gas-phase cross sections, such as those discussed in this thesis, are only a first-order approximation to those for the true *in vivo* situation. Accurate studies aiming at faithfully reproducing the tracks of particles moving in the human body would clearly require data in the condensed phase (Plante and Cucinotta, 2009). Nonetheless, as such data is currently unavailable, corresponding gas phase results are the best available alternative at this time and represent a good starting point for simulations devoted to the development of energy deposition models at the molecular level (Muñoz *et al.*, 2007). White and Robson (2009) have recently proposed a kinetic transport model, in which cross sections for scattering from single molecules are blended with a structure function of the medium as a whole; this approach may provide a connection between the gas phase and the *in vivo* conditions.

From the picture outlined so far, it should be pretty clear as to why it is especially interesting to study the interaction between positrons and those molecules that can be considered as the components or “building blocks” of the nucleic acids. Applications to biomedical research are of course not the only motivation for investigating these kind of targets, since exploring the fundamental forces driving the dynamics of the scattering processes is still of primary interest to the ATMOP community. Hence, it is not too surprising that significant recent work has been devoted to studying targets that include both the applications and fundamental scattering phenomena.

Unfortunately, at least in part owing to the practical difficulties in producing a molecular beam or target cell of pure DNA, it is not always

possible to directly study the biomolecules of interest. Moreover, most of the nucleobases are solid targets at room temperature, which makes them somewhat hard to experimentally measure with the currently available beamlines. So, the ATMOP community has recently focussed its interest into a class of organic compounds that can be thought of as sub-units or moieties to the nucleotides, and more in general to the components of nucleic acids in living matter. The reductionist philosophy whereby the physical, chemical and biological properties of a system stem from the fundamental properties of its constituents and their interactions appears to have been now accepted in the field (see e.g. Ptasińska *et al.*, 2004; Abdoul-Carime *et al.*, 2004; Bouchiha *et al.*, 2007; Giardini *et al.*, 2005).

The aim of this chapter is to present and discuss new positron cross section measurements for six targets that are of particular biological interest to the ATMOP community for the reasons canvassed above. These molecules are formic acid (HCOOH), tetrahydrofuran (THF, C₄H₈O), 3-hydroxy-tetrahydrofuran (3H-THF, C₄H₈O₂), tetrahydrofurfuryl alcohol (THFA, C₅H₁₀O₂), 3,4-dihydropyran (DHP, C₅H₈O) and pyrimidine (C₄H₄N₂). A schematic diagram of their respective structures is given in Fig. 6.1. We note that some of these molecules are very similar in their structure. In organic chemistry, structurally related molecules are often studied to better understand corresponding trends in their chemical activity. Such studies are not so widespread in physics, although we note the extensive positron annihilation work by Surko *et al.* (2005) on the alkane (C_nH_{2n+2}) homologous series, whose observed structures could be associated to the presence of vibrational Feshbach resonances. An analogous positron annihilation study, but this time on the fluorinated methane series CH_nF_{4-n}, was conducted again by the San Diego group (Barnes *et al.*, 2003). Investigations of positron-molecule collisions, in which TCSs for a series of structurally related species are measured, are instead much more limited. We mention, however, the review study by Kimura *et al.* (2000) and the work of Zecca *et al.* (2007).

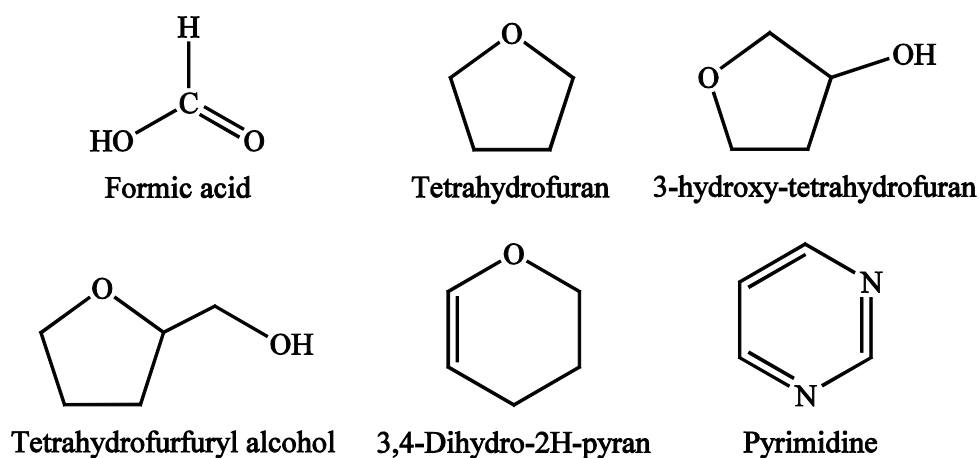


Fig. 6.1. Schematic diagram of the structure of the molecules of biological interest under investigation in the present thesis.

The results presented in this chapter consist of total cross sections for all the molecules of Fig. 6.1, except tetrahydrofuran, which were measured with the Trento spectrometer. Total, positronium formation and elastic differential cross sections for tetrahydrofuran, instead, were collected with the ANU apparatus. At the end of this chapter we also seek to investigate if there are any trends in the energy dependence of the TCSs for all these species, and if so can those trends be related to some of the most important physico-chemical properties of the molecules in question.

6.2 Formic acid

In this section we report on TCS measurements for positron scattering from the important molecule formic acid, which were undertaken with the Trento apparatus. Formic acid (chemical formula HCOOH) is the simplest organic acid and the simplest acid containing a carboxyl functional group ($-\text{COOH}$) (see Fig. 6.1). Owing to its important role as an intermediate in chemical synthesis, formic acid is a fundamental molecule in the process of formation of larger biomolecules such as glycine and acetic acid. More complex biomolecules, including some of the amino acids, indeed, originate from the formate group ($-\text{COOH}$) of the formic acid molecule. Amino acids are the component units of the single linear polymer chains known as proteins, the latter being one of the three major macromolecules, together with the nucleic acids DNA and RNA, that play a vital role in the biological processes at the base of all known forms of life.

Formic acid represents also an intriguing system to investigate positron scattering from a fundamental point of view. It has a large permanent dipole moment $\mu = 1.41$ D (Lide, 1998) and a somewhat significant dipole polarisability $\alpha = 22.5$ a.u. (Vizcaino *et al.*, 2006). It is also a quite small molecule (hard sphere size $D = 3.8$ Å; Vizcaino *et al.*, 2006), which should make attempts to perform quite sophisticated calculations somewhat easier. Scattering models need to account for these and other physical effects. It is well known that, at low energy, the overall potential experienced by the positron during the collision with the molecules originates from the sum of the attractive (negative) polarisability interaction and the repulsive (positive) static mean field (Surko *et al.*, 2005). So, if both potentials are, for example, of the same magnitude, the offset between the two depends to a great extent on the details of the calculated potentials, i.e. how they effectively reproduce the real interactions in the model.

It is therefore not surprising that there has been significant recent interest in formic acid, with diverse research on electron scattering from this species being available in the literature. These studies have examined formic acid both from an experimental (Pelc *et al.*, 2002; Prabhudesai *et al.*, 2005; Vizcaino *et al.*, 2006; Nixon *et al.*, 2008; Allan, 2006) as well as from a theoretical perspective (Gianturco and Lucchese, 2006; Trevisan *et al.*, 2006; Rescigno *et al.*, 2006; Bettega, 2006), and have focussed on its dissociation dynamics, absolute cross-section measurements and vibrational excitation analyses.

On the other hand, the knowledge with respect to positron scattering from formic acid is rather limited, as compared with the electron case. Positron impact experiments on formic acid have been reported in the paper by Kimura *et al.* (2000) and, more recently by Makochekanwa *et al.* (2009), who measured not only the total cross sections, but also the positronium formation cross sections. The only theoretical calculation on the positron-formic acid system was carried out by the Brazilian group of Bettega and Lima (Zecca *et al.*, 2008c). Hence, accurate experimental data can be very useful in assisting the development and validation of theory, especially in the very low energy range below ~ 1 eV, where basically no experimental data was available prior to this investigation.

6.2.1 Experimental details

The present experiment on formic acid was carried out according to the procedure outlined in Section 2.1 for the Trento apparatus and by employing a high-purity target sample ($\sim 98\%$, Aldrich). We note that formic acid presents some experimental challenges: at room temperature it consists of a mixture of both its monomer and dimer forms, with the degree of dimerization depending on the pressure and temperature of the sample (Coolidge, 1928). The fraction of monomer/dimer composition in the target can be easily calculated following the prescription of Taylor and Bruton (1952). The results of such a computation are given in Fig. 6.2, where the percentage of the dimer in the sample is given as a function of pressure, at constant room temperature (~ 24 °C). Fig. 6.2 shows that for the typical sample pressures of this study (10^{-3} - 10^{-4} Torr), a beam composition of $\leq 5\%$ dimer and $\geq 95\%$ monomer is to be expected, so that the measured TCSs represent an average for that ensemble. The formic acid monomer has also two stable planar forms, the *cis* and *trans* isomers and the energy difference between the two isomers in the gas phase amounts to 0.169 eV (Vizcaino *et al.*, 2006). An estimate of the population ratio at room temperature based on the Boltzmann distribution demonstrates a clear predominance of the *trans* form (~ 1000 times more abundant) in our sample, so that the effect of the *cis* form can be neglected here.

For this experiment the pressure readings of the gas vapour and the background vacuum inside the scattering cell were achieved with the 628B model Baratron, whose operating temperature is 100 °C. The temperature of the target gas in the scattering region was assumed to remain nearly constant during the different runs and to be close to the room temperature ($\sim 25 \pm 2$ °C). Owing to the temperature gradient between the formic acid vapour in the scattering cell and the manometer operating temperature, the pressure readings had to be corrected for the thermal transpiration effect. This was done by using Eq. (2.15) with $D = 3.8$ Å (Vizcaino *et al.*, 2006) as the estimate of the formic acid molecular diameter. The thermal transpiration correction was less than +10% in terms of the change of the TCS magnitude over the entire positron energy range.

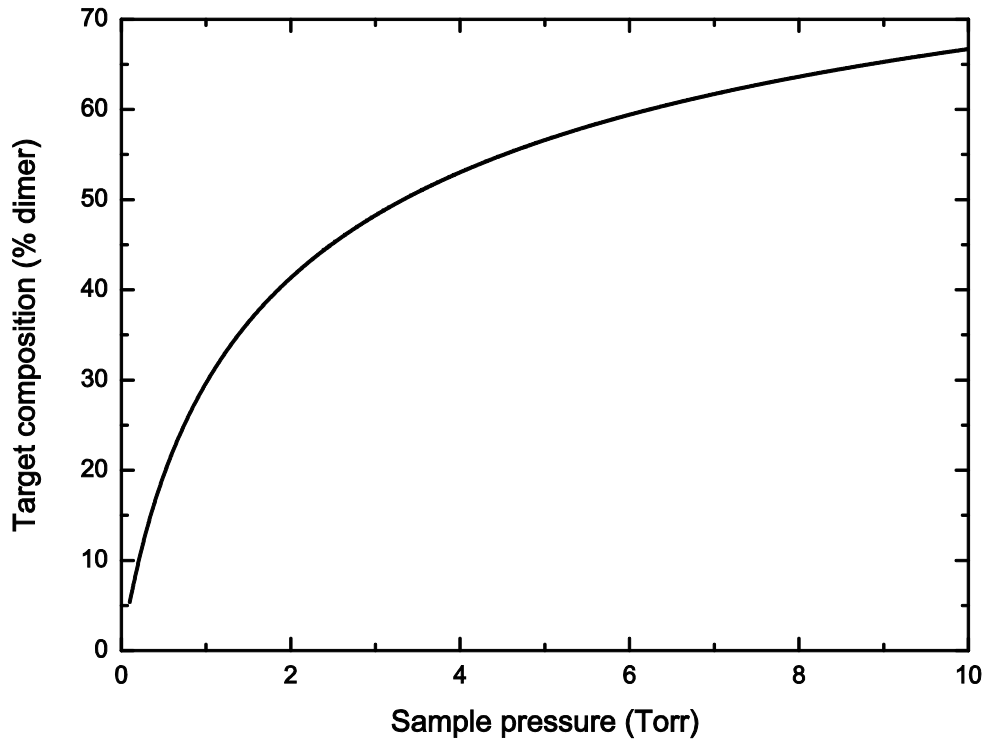


Fig. 6.2. The percentage of dimer target composition in formic acid as a function of pressure at room temperature (24 °C).

The intensity of the focussing axial magnetic field present in the scattering region was kept between ~ 8 and ~ 10 G during this experiment. This led to a correction in the positrons effective path length L , due to the gyration of the particles in the scattering region, of $\sim 5\%$. As we observed in Section 2.1.3.4, the gyration of the projectile particles can also potentially increase the angular resolution error with respect to the no-field case (Hamada and Sueoka, 1994). The present TCSs could in principle be corrected for this angular discrimination effect, given the estimates of the energy-dependent angular discrimination of the Trento apparatus (Table 2.5) and provided appropriate absolute elastic differential cross sections are available at each energy. We note that experimental differential cross sections for formic acid are currently unavailable, whereas theoretical differential cross sections, although not readily available in the literature, would be accessible as a result of the calculations by the Brazilian group (Zecca *et al.*, 2008c). Indeed, Makochekanwa *et al.* (2009) have used those DCSs to correct their TCSs for the angular discrimination effect. Of course we could use the same elastic DCSs in a similar manner to that in Makochekanwa *et al.* (2009) to correct the present TCSs for the forward scattering effect. However, as we shall see below, there is only qualitative (shape) accord between our measured TCSs and the calculated elastic ICSs. We therefore think that employing those DCS in this manner would be a little premature at this time and so we have chosen not to make such a correction to our measured TCS. As a consequence, the TCSs we report here represent a lower bound on the “real” values. A quantitative discussion

of the experimental angular discrimination and its effect on measured TCSs has been recently published in the paper by Sullivan *et al.* (2011), so that the reader can refer to this reference for more information.

When this experiment was carried out, the radioactive ^{22}Na isotope had an activity of approximately 3.9 mCi and the energy width of the positron beam was evaluated to be ~ 0.3 eV, as a 1 μm -thick tungsten moderator was in use. This implies that the measured TCSs at the lowest positron energies are affected by the convolution over this energy resolution. The real TCSs below a fraction of an eV would thus actually be somewhat higher in magnitude than what we report here, once they had been corrected for this effect (refer to Section 2.1.2.2 for more details).

6.2.2 Results and discussion

The measured TCSs for positron scattering from formic acid are given in Table 6.1 and are shown in Figs. 6.3 and 6.4. The energy range covered in the experiment on this target is 0.3-50.2 eV. The statistical uncertainties on the TCS results were calculated as one standard deviation of the average of many runs carried out at the same energy: these errors are given for each energy value in Table 6.1 along with the corresponding TCS average. The statistical errors on the present data amount to about 3% on average, but generally span the ~ 1 -5% range over the energies covered in the present experiment. The absolute uncertainties on the present results (not given in Table 6.1) were evaluated as the root of the quadratic sum of the individual contributing errors, including the statistical component. The overall errors are in the ~ 5 -9% range, with the biggest values occurring only at the lowest energies.

Fig. 6.3 shows that the positron-formic acid TCS decreases monotonically with a $\sim 1/E$ energy dependence up to about the positronium formation threshold. The shape and magnitude of the low energy cross section clearly shows the importance of both the dipole polarisability and permanent dipole moment of the target on the scattering processes taking place, in that energy range. This is consistent with the corresponding electron scattering results on this target molecule (see e.g. Brunger *et al.*, 2009).

The effect of the opening of the positronium formation and then, albeit to a lesser degree, direct ionisation channels is manifest on the shape of the TCS and is clearly seen as a change in the slope of the TCS in close proximity to the corresponding energy thresholds (see Fig. 6.3). With the aim of determining the positronium formation threshold for formic acid from our TCS results, in Fig. 6.3 we also draw lines of best fit, to try and highlight at about what energy the TCS changes its slope. The lines in question are the least-squares fits to the two subsets of points on the right and left side of the graph (i.e. before and after the energy threshold of interest), where that division is chosen to give the largest ratio of the slope on the left to the slope on the right, subject to the condition that each subset contains at least 10 points. We find that this circumstance is satisfied when the first subset of points includes the energies from 0.3 to 4.7 eV and the

second one spans the data in the range 5.2-50.2 eV. In this case, the intersection between the two best fit lines occurs at $\sim 4.3 \pm 0.3$ eV. As the first ionisation potential (IP) for the formic acid monomer and dimer is 11.4 ± 0.2 eV (Lide, 1998), and as in general the positronium formation threshold (Ps) of a species can be obtained from its ionisation potential using Eq. (3.1), we find that $Ps = 4.6 \pm 0.2$ eV for formic acid. This value for the positronium threshold is consistent with the one that we have derived from the data of Fig. 6.3, so that the energy where the TCS changes slope is indeed indicative for the positronium channel becoming open.

Table 6.1. The present total cross sections for positron scattering from formic acid. The errors represent only the statistical components of the overall uncertainties and are at the one standard deviation level ($\pm 1\sigma$).

Energy (eV)	TCS (10^{-20} m^2)		Energy (eV)	TCS (10^{-20} m^2)	
	Average	Error		Average	Error
0.30	161.00	10.60	6.95	17.10	0.40
0.35	154.90	13.80	7.20	16.20	0.50
0.40	113.20	7.60	7.45	15.70	0.60
0.50	109.10	11.90	7.70	16.80	0.50
0.60	82.20	5.30	7.95	16.40	0.10
0.70	70.80	4.20	8.20	16.30	0.40
0.80	62.10	3.60	8.45	16.30	0.10
0.90	57.30	1.30	8.70	16.20	0.60
1.00	49.50	1.90	9.20	16.30	0.40
1.10	48.10	3.20	9.70	16.60	0.20
1.20	46.50	1.80	10.20	16.10	0.20
1.30	44.90	1.10	11.20	16.10	0.10
1.60	36.30	1.90	12.20	15.90	0.20
1.80	31.60	1.20	13.20	15.60	0.60
2.20	28.90	0.80	14.20	15.10	0.10
2.70	25.70	1.00	15.20	15.40	0.10
3.20	22.20	0.50	16.70	14.80	0.20
3.70	21.50	1.40	20.20	14.80	0.20
4.20	19.10	1.00	22.20	14.40	0.20
4.45	18.70	0.60	24.70	14.80	0.10
4.70	18.30	0.70	28.20	14.60	0.10
5.20	17.90	0.40	31.70	14.30	0.40
5.45	17.80	0.10	37.70	14.00	0.30
5.70	17.10	0.30	40.20	13.70	0.10
5.95	17.00	0.30	43.20	13.20	0.20
6.20	16.80	0.60	45.20	12.90	0.40
6.45	16.50	0.10	50.20	12.50	0.30
6.70	16.60	0.40			

The only published theoretical investigation into positron scattering from formic acid is the study by the Brazilian group of Bettega and Lima, that can

be found in the paper by Zecca *et al.* (2008c). In that paper elastic integral cross sections are given for the formic acid monomer only, by employing the Schwinger multichannel method (SMC), a technique that was developed for electron scattering, but that was later extended for studying positron-molecule collisions (Germano and Lima, 1993; da Silva *et al.*, 1994; 1996; 1998). The theoretical results are presented at different levels of complexity, namely at the static, static plus polarisation, static plus Born closure and static plus polarisation plus Born-closure levels. From the experimental side, there is in the literature only a couple of other experimental positron impact works on formic acid: these were carried out by the groups at Yamaguchi University (Kimura *et al.*, 2000) and at the Australian National University (Makochekanwa *et al.*, 2009).

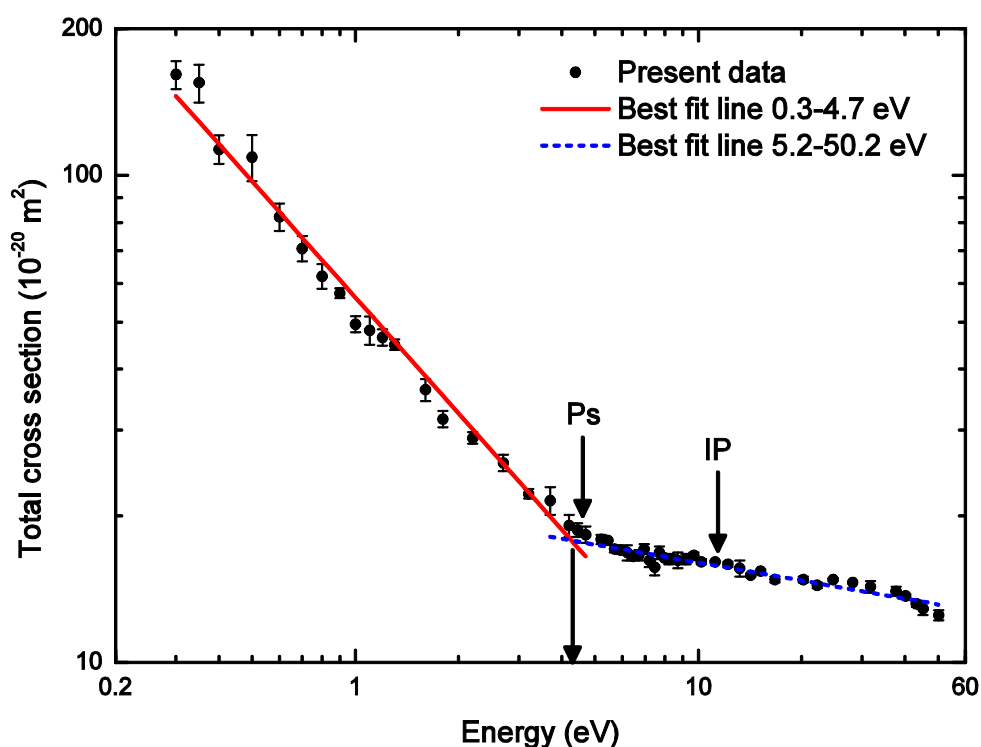


Fig. 6.3. The present total cross sections for positron scattering from formic acid. The positronium formation threshold (Ps) and the first ionisation potential (IP) are indicated by labelled arrows. Also drawn are least-squares linear fits to the two subsets of points in the energy range 0.3-4.7 eV and 5.2-50.2 eV. The vertical black arrow indicates the energy value where the two lines intersect.

In Fig. 6.4 the present experimental results are compared with the theoretical calculations in Zecca *et al.* (2008c) and the experimental data by Makochekanwa *et al.* (2009) and Kimura *et al.* (2000). Let us first discuss the comparison between the present data and the computations presented in Zecca *et al.* (2008c). We will limit the discussion of the theoretical calculations to below the positronium formation threshold, as the SMC

calculations do not incorporate the scattering channels corresponding to positronium formation, direct ionisation and the electronic excitation states. The theoretical results, including an accurate model for the target polarisation, are shown only for energies up to ~ 10 eV, since for higher energies the results with polarisation display several pseudo-resonances that may be due to the closed channels that should be open at those energies (Zecca *et al.*, 2008c). We note in Fig. 6.4 that the calculated elastic integral cross sections qualitatively follows the measured TCSs for most energies. When the calculation accounts for the static and static plus polarisation approximation only, without considering the Born-closure, the theoretical results are found to lie below the experimental data. With the inclusion of Born-closure, the calculated cross sections become larger than the experimental cross sections at almost all energies.

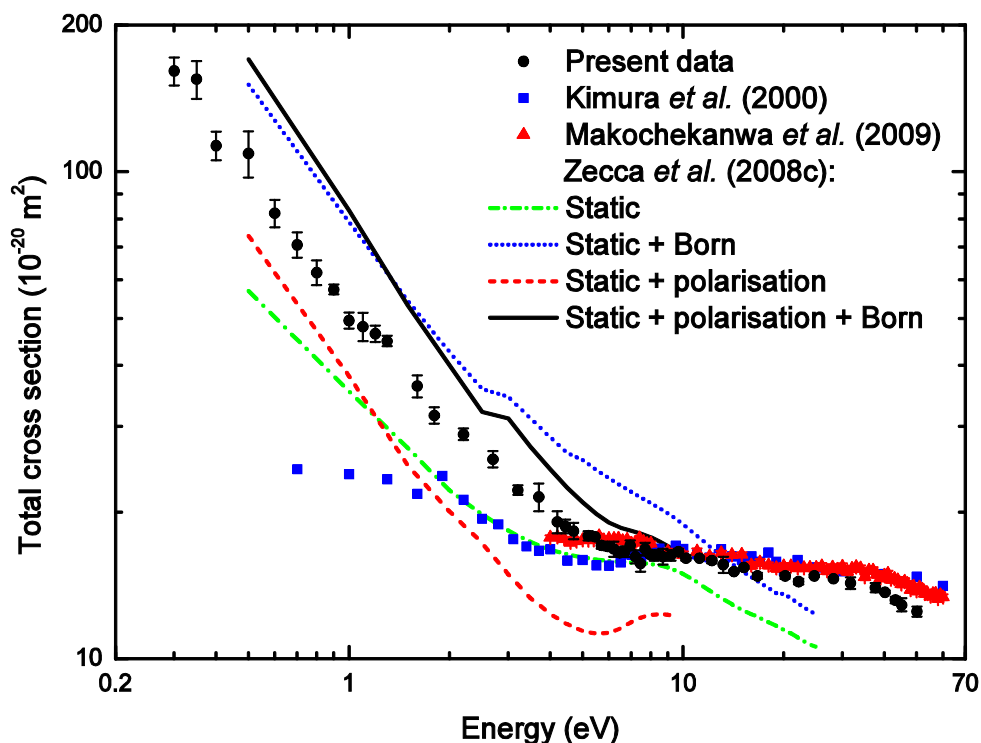


Fig. 6.4. The present total cross sections for positron scattering from formic acid are compared with the calculations of the elastic integral cross section by Zecca *et al.* (2008c), at different levels of physical modelling of the scattering process, and with the experimental results by Makochekanwa *et al.* (2009) and Kimura *et al.* (2000).

As the elastic SMC calculation including the static, polarisation, and Born-closure dipole interactions (black line in Fig. 6.4) is the most accurate and physical representation of the scattering process, we limit the discussion to a quantitative comparison between it and our experimental TCS results. We immediately note that of course it is unphysical for an elastic integral cross section to be greater in magnitude than the corresponding TCS, which

is exactly what happens in Fig. 6.4. However, there are four possible reasons for why this can occur, all of which might at least in part be responsible for this apparent inconsistency. First, as we have discussed in the previous Section, the present TCSs are not corrected for forward angle scattering effects. If such a correction were to be applied, it would only make the magnitude of the experimental TCS increase, especially at the lower energies where the angular discrimination is larger, thereby reducing, at least in part, the discrepancy between theory and experiment. Secondly, in the experiment the sample target was a mixture of formic acid monomer and dimer, while the calculation was performed for the monomer alone. This too could partially account for the magnitude discrepancy between our measurement and the most physical elastic ICS calculation. However, now for electron scattering from formic acid, Gianturco and Lucchese (2006) found that the elastic cross sections for the dimer alone tended to be somewhat larger in magnitude than the corresponding results for the monomer. So if this was the case for the antiparticle counterpart as well, it would actually increase the observed disparity; nevertheless, this effect is yet to be quantified for positron scattering. Moreover, as the fraction of dimer in the sample is relatively small at the typical pressures employed in the present experiment, we would expect this correction to have only a second order effect on the TCS magnitude. Thirdly we note that in the experiment, the formic acid sample exists in a distribution of allowed rotational states (j), given by the Boltzmann distribution, whereas the computation is for scattering from only the initial state $j = 0$. This difference might therefore also explain some of the discrepancy observed in Fig. 6.4 between our measurements and the calculations. Finally, it is well known that the Born-closure approach somewhat overestimates the lower-energy values of the elastic integral cross section (Bouchiha *et al.*, 2007), as the corresponding differential cross section, that typically becomes more forward peaked when going to lower energies, diverges in the very forward angle direction. This effect has already been observed by Bouchiha *et al.* (2007) in their elastic R -matrix electron-methanol results when compared to the experimental total cross section data (Szmytkowski and Krzysztofowicz, 1995).

Let us compare now the present formic acid data with the other positron experimental results available in the literature (Fig. 6.4). The agreement with the data by Kimura *et al.* (2000), spanning the 0.7-600 eV energy range, is pretty good, to within the combined errors, for the overlapping high energies down to ~ 6 eV. Below that energy, the data of Kimura *et al.* (2000) underestimates the magnitude of the present TCS, with the discrepancy progressively increasing towards the lowest energies. Now, this appears to be quite a systematic observation, when comparing TCSs for a target that has been independently measured with the Trento apparatus and that of Yamaguchi University. In fact, in this thesis we have already observed this same feature in the TCSs for the isoelectronic molecules N_2 , CO and C_2H_2 (see Chapter 4) and methanol (see Chapter 5). As we have explained in those cases, the low energy discrepancy in the TCS magnitude is possibly due to the present apparatus having a better angular

discrimination (which we remind the reader is energy dependent) compared to that of the spectrometer employed at Yamaguchi University for experiments on the same molecules.

In respect to the more recent measurements by the ANU group on formic acid (Makochekanwa *et al.*, 2009), we observe that their data shown in Fig. 6.4 ranges from 4 eV to 60 eV positron energy and is uncorrected for the forward angle scattering effect. However, we also note that the ANU group employed estimates of their missing angles for that experiment, together with the elastic DCSs stemming from the SMC calculations of the Brazilian group, to quantify the effect of the forward scattering correction on their measured TCSs (Makochekanwa *et al.*, 2009). They found that the TCS measured with their apparatus should be increased by 45% at 4 eV positron energy to account for this effect, and that the forward angle scattering correction becomes negligible only above 15 eV (Makochekanwa *et al.*, 2009). However, since the present TCSs are uncorrected for this same effect, for the reason outlined above, we compare our results only to the ANU uncorrected data shown in Fig. 6.4. In this case, we find a good agreement, to within the combined total if not just statistical error bars, between the two data sets in the entire energy range of overlap.

Finally, we note that although the electron-formic acid elastic collision cross section shows a shape resonance in the A'' symmetry (Allan, 2006; Trevisan *et al.*, 2006; Bettega, 2006; Rescigno *et al.*, 2006), the present positron cross section appears to be structureless. We do not see such a resonance with positrons basically because the short-range potential seen by the incoming positron is dominated by the repulsive nuclear potential. Therefore, the resulting potential (short range plus angular momentum barrier) would not be able to support a shape resonance.

6.3 Tetrahydrofuran

This section presents the results of the experiments for positron scattering from the tetrahydrofuran. This molecule was investigated using the atomic and molecular positron beamline at the Australian National University.

Tetrahydrofuran (THF, C_4H_8O) is a heterocyclic organic compound containing an ether group (Fig. 6.1). It has an exposed oxygen atom available for hydrogen bonding, which makes THF fairly miscible in water and one of the most polar simple ethers. The THF molecule is a five-atom ring that, however, is known to come in three symmetric forms and two asymmetric forms (Cadioli *et al.*, 1993). The structures of the three conformational isomers, which differ in their geometrical symmetries, are schematically shown in Fig. 6.5 and are known as C_2 (1 π -rotation axis), C_s (1 reflection plane) and C_{2v} (1 π -rotation axis and 2 vertical mirror planes) (Winstead and McKoy, 2006). In the C_{2v} geometry, the four carbon atoms and the oxygen atom form a planar ring. An elaborate calculation of the energy minima points to C_s as the most stable conformer among the three (Rayón and Sordo, 2005), although other computations place the C_2 minimum slightly below that of C_s (Cadioli *et al.*, 1993; Winstead and

McKoy, 2006). The C_{2v} geometry, instead, seems to lie in any case above both the C_2 and C_s energy minima (Rayón and Sordo, 2005; Winstead and McKoy, 2006). Nonetheless, the energy difference in the ground state between the three conformers is very small (Winstead and McKoy, 2006; Cadioli *et al.*, 1993).

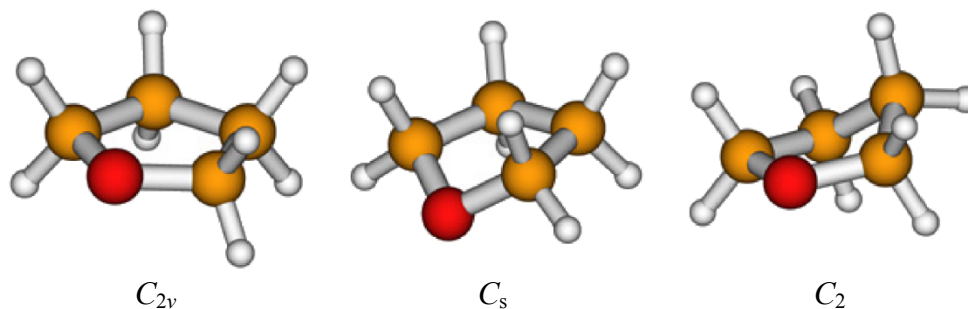


Fig. 6.5. Schematic diagrams of the energy minima structures of the three symmetric conformers of tetrahydrofuran (Winstead and McKoy, 2006).

THF is a very common organic solvent which is used in large amounts for a variety of industrial purposes (Thiemer *et al.*, 2003), although its main application is as a precursor to linear polymers, like polytetramethylene oxide (PTMO). As a consequence, many of the early studies on its properties aimed at understanding its geometry and vibrational spectra, mainly by infrared and Raman spectroscopies and computational means (Palm and Bissel, 1960; Eyster and Prohofsky, 1974; David and Ibberson, 1992; Gallinella *et al.*, 1974).

More recently, however, THF obtained some new interest, when the scientific community realized that it can be considered as a prototypical building block for living matter (Antic *et al.*, 1999), because of its similarity to the pyrimidine-based nucleobases. As a model for the sugar rings in the nucleic acids, it also plays an important role as a component in the structure of both DNA (Lepage *et al.*, 1998; Antic *et al.*, 2000; Milosavljević *et al.*, 2004) and RNA (Thiemer *et al.*, 2003; <http://www.proligo.com>). The backbone of DNA can, in fact, be viewed as a series of THF and 3-hydroxy-tetrahydrofuran (3H-THF) molecules held together by phosphate bonds to which the nucleobases are covalently linked (see Fig. 6.6). We also note the importance of the THF moiety in the metabolism of the HIV (AIDS) inhibitor agenerase (<http://www.aidsmed.com>) in the human liver.

As the high-energy ionising radiation entering biological matter is ultimately channelled into the production of numerous low-energy secondary electrons, most scattering experiments in the last decade or so have concentrated on resonant electron measurements from solid and gas phase DNA constituents (Lepage *et al.*, 1998; Antic *et al.*, 2000; Milosavljević *et al.*, 2004; Huels *et al.*, 1998), although for completeness we also note the helium atom scattering work from Gebauer *et al.* (1997). In effect, several impact experiments on THF (Zecca *et al.*, 2005; Możejko *et al.*, 2006b; Aflatooni *et al.*, 2006; Milosavljević *et al.*, 2005; Dampc *et al.*,

2007a; 2007b; Colyer *et al.*, 2007; Allan, 2007) have been recently carried out with electrons as a probe. This can be explained, at least in part, in terms of a search for resonances in the vibrational excitation (Allan, 2007; Dampc *et al.*, 2007a) or dissociative electron attachment (Aflatooni *et al.*, 2006) channels that might constitute an initial step to better understand the details of energy deposition by ionising radiation in DNA (Zecca *et al.*, 2005).

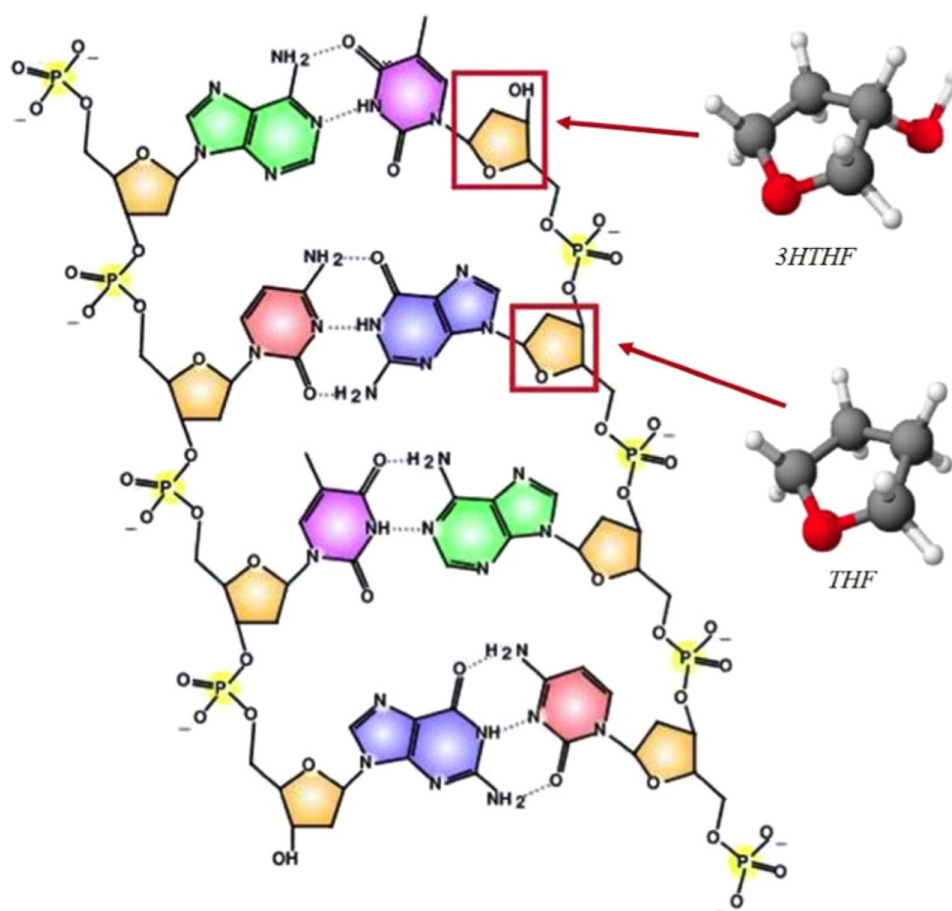


Fig. 6.6. Schematic diagram of an unrolled segment of DNA, with the tetrahydrofuran (THF) and 3-hydroxy-tetrahydrofuran (3H-THF) components highlighted. Also shown are geometrical representations for the global energy minima structures of both species.

The only previous experimental study that we know of, employing positrons as the projectile particle for scattering experiments from this species, is that of Zecca *et al.* (2005). Those authors reported in the same paper low resolution electron- and relatively high resolution positron-TCSs in the energy range ~ 0.1 -20 eV, that had been measured with the apparatus at Trento University. On the theoretical side, there is no evidence for any positron calculation on THF having been completed so far. This possibly reflects the complexity involved in modelling this kind of target, as well as the problems related to being able to introduce into the calculation the

different scattering channels (positronium formation, ionisation, electronic excitation, vibrations, rotations, etc.) that are open at the typical energies of the present investigation.

In this section we present new positron-THF TCS results that have been collected at ANU with a higher energy resolution compared to those of Zecca *et al.* (2005). In addition, positronium formation cross sections and some elastic differential cross sections at selected positron impact energies have also been measured as part of this same investigation. Discussion for the contribution of the inelastic channels to the total scattering is also provided.

6.3.1 Experimental details

The results of the measurements on THF described in the following section have been obtained by using the ANU positron beamline. The experimental procedures and techniques usually employed when using that apparatus have already been described in Section 2.2, so that here we need to give only some details pertaining to these specific experiments.

First of all, throughout all the current measurements we used a high-purity THF sample, containing a 0.1% maximum impurity of water and stabilised with 0.04% of butylated hydroxytoluene (DuPont). Although THF is liquid at room temperature, it is volatile enough (vapour pressure $P = 176$ hPa at 25 °C; NIOSH, 2007) to provide an adequate amount of vapour to carry out beam attenuation measurements in our experiments. Note that THF is rather hygroscopic (Zecca *et al.*, 2005), so once decanted into the sample holder, we have performed various freeze-pump-thaw cycles, in order to degas the target sample and remove any impurities present in that sample that may affect the results of the measurements.

The THF pressure in the scattering cell was set to be in the range $1\text{--}4 \times 10^{-4}$ Torr during the present measurements. Since the target vapour was assumed to be at room temperature ($\sim 24 \pm 2$ °C), whereas the pressure in the scattering cell was measured with a Baratron operating at 45 °C, the pressure readings had to be corrected for the thermal transpiration effect by following the procedure outlined in section 2.1.3.2 (see also Section 2.2.3.5). In order to do so, we employed the estimate of the hard-sphere diameter for the THF molecule $D = 4.63$ Å, as suggested by Dampc *et al.* (2007b). This correction turned out to be a maximum of $\sim +3\%$ on the magnitude of the cross sections for all the experiments described here.

The buffer-gas trap settings we employed in our experiments are summarised in Table 6.2 and shown graphically in Fig. 6.7: there the electrode potentials in each trap stage and the time duration of the various stages are given. These specific settings have been used for all the experiments described in this section. The beam transport energy (and consequently a few other electrode voltages during the dump stage), however, had to be changed sometimes: this was either set to 25 eV, 50 eV or 60 eV, depending on the energy range scanned during a specific run. The moderator potential was set to 18.8 V and was kept constant. The rotating

wall was used in continuous mode, with its frequency and amplitude set to 4.2 Mhz and 100%, respectively.

Table 6.2. The present buffer-gas trap settings. The time of the load, cool and dump stages are given together with the potential on the electrodes during each trap stage. Note that the E7, E8 and E9 electrodes in the dump stage were set to one of the three potentials shown here for the different measurements.

		Stage				
		Load	Cool	Dump		
Potential (V)	Time (ms)	9.5	2	1		
	E1	15	15	15	15	
E2	10	10	10	10		
E3	10	10	10	10		
E4	10	10	10	10		
E5	10	10	10	10		
E6	10	10	10	10		
E7	10	35	35	60	70	70
E8	1	1	25.5	50.5	60.5	60.5
E9	35	35	25	50	60	60

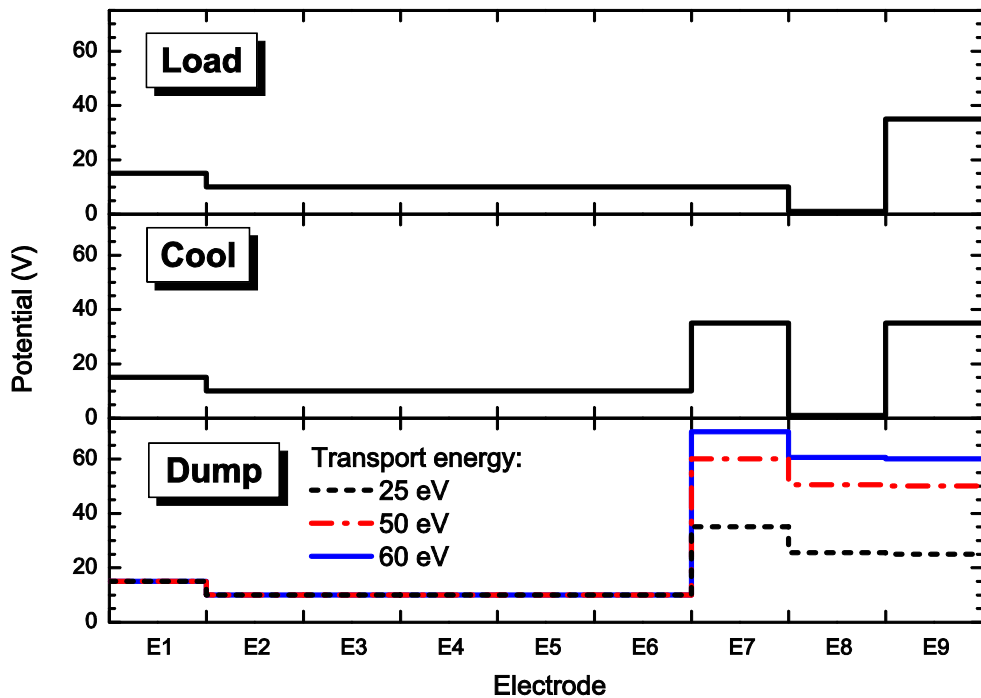


Fig. 6.7. Schematic plot of the different electrode potentials set during the trap stages of the present measurements. Note that three different transport energies were employed for the current experiments (25 eV, 50 eV, or 60 eV), so that three different potential configurations of the E7, E8 and E9 electrodes during the dump stage were alternately used.

The energy resolution of the positron beam was, on average, 61 meV (FWHM), however, it was found to vary between 41 and 72 meV during the various present measurements. This variation is most likely due to discrepancies in the performance of the various Ne moderators employed during the different experiments, as the trap settings were basically kept constant. Note, in fact, that in order to work with a sufficiently large amplitude for the positron pulse area, the moderator had to be grown again every 2 to 4 days. Differences in the moderator performance can ultimately be traced back to microscopic differences arising in the Ne crystallisation process during the moderator growth phase, which may affect not only the energy spread of the emitted positrons, but also the moderation efficiency. Another possible factor affecting the energy resolution is the background pressure in the source chamber during the moderator growing phase, which can slightly fluctuate from one experiment to another. Nevertheless, these changes in the energy width were found not to have a significant impact on the results of our cross section measurements, except for changing the missing angle range affecting the various measurements (see Eq. 2.44). Owing to the relatively high energy resolution that can be achieved with this buffer-gas trap-based apparatus and given that the lowest positron energy reached in these experiments is ~ 1 eV, the convolution effect due to the finite energy resolution of the beam over the measured cross sections is expected to be negligible here. In any case the exact cross sections would actually only be slightly different in magnitude than what are reported here, if they were corrected for this effect. Note that as this effect is shape dependent, the correction would be different for dissimilar cross sections.

As specifically explained in Section 2.2.3.2, in order to separate the inelastic scattering channels from the elastic channel, we have employed a beach ratio $M > 1$ during some of our measurements. In particular, the total and positronium formation cross sections and the elastic differential cross sections in the energy range 1-6 eV were measured without a beach ($M = 1$), while the elastic differential cross sections, spanning 8-25 eV, were measured by employing a beach ($M = 5$). The reasons for these choices are explained in the following text.

The total cross section can in principle be measured with any value of $M \geq 1$. However, we know that the elastic scattering cross sections suffer from some angular discrimination limitations (see Section 2.2.3.3) that vary with the value of M . The greater is M , the larger will be the missing angle range affecting the elastic DCS measurements (see below), hence, resulting in lower magnitude elastic integral cross sections in the corresponding range of acceptable angles. This means that the total cross section magnitude becomes lower with increasing M value and this effect is typically greatest at the lowest energies, where the missing angle range is larger (see again Section 2.2.3.3 and below). In other words, the presence of a beach greatly amplifies the forward angle scattering effect and so the best choice to minimise the correction for this effect is to employ $M = 1$ for the TCS. In addition, with $M = 1$ the energy-dependent angular discrimination, and therefore the correction for the forward angle scattering effect for a given molecule, of the ANU apparatus is very similar to that of the Trento

apparatus (see Chapter 2). This allows us to easily compare the TCS results for the same species as measured with the two beamlines.

Positronium formation is an inelastic loss process for the incoming positron, and thus the cross section measurements for this scattering channel are not affected by angular discrimination effect. Hence, the most obvious choice is to employ again $M = 1$ in this case.

On the contrary, to separate out the elastic channel from the inelastic channels a beach has to be used. This is the case for the “elastic” differential cross sections measured above the threshold of the first inelastic process, i.e. the first electronic excited state. Please note that it would be more correct to define them as quasi-elastic DCSs, as they include also vibrational and rotational channels. These vibrational scattering channels could, in principle, also be separated from that for elastic scattering by employing a larger beach ratio. However, unfortunately, this is currently not feasible. Nevertheless, the magnitude of the cross sections for these channels is expected to be very small compared to that of the purely elastic channel, so that their contribution to the elastic DCSs should be negligible or within the empirical uncertainties. It is known that the energy of the first electronic state (1B_1) in THF (Bouchiha *et al.*, 2006) that can be excited by positrons is $E_{\text{exc}} = 6.57$ eV (Tam and Brion, 1974). Hence, the measurement of elastic DCSs at energies below that threshold does not require a beach ($M = 1$), as elastic scattering is basically the only open channel (except for vibrations, rotations and positronium formation, which is a loss process). The elastic DCS measurements at energies higher than that threshold, instead, do need a beach in order to remove the inelastic processes. We used a beach ratio of $M = 5$, so that we could potentially make measurements of elastic DCSs at energies up to:

$$E = M \times E_{\text{exc}} = 5 \times 6.57 \text{ eV} = 32.85 \text{ eV}, \quad (6.3)$$

without including any contribution from inelastic processes like electronic excitations or direct ionisation.

Note that despite the consequent experimental limitations (i.e. larger missing angles), total and positronium cross sections, and elastic differential cross sections below the energy threshold of the first excited state, can still be measured with a beach. Indeed we have carried out a few of these specific measurements with $M = 5$ to check for the consistency of the measurements with different M values. Although not shown in the next section, we have found that, for instance, the positronium formation cross section measured with $M = 1$ is in very good agreement with that measured with $M = 5$, as we had expected. The elastic DCS at 5 eV energy measured with $M = 1$, although presenting much smaller missing angles compared to the same DCS measured with $M = 5$, agrees with it over the common range of accessible scattering angles, again as we would have anticipated from the discussion outlined above.

The angular discrimination, affecting the present TCSs and elastic DCSs, has been estimated as a function of the scattering energy by using Eq. (2.44) with the corresponding M ratio employed during that experiment and the

energy resolution ΔE of the beam at that time. These results are reported in Tables 6.3 and 6.4, respectively, for selected positron energies. The angular discrimination of the present TCS results lies in the range $\theta_{\min} = 1.7^\circ$ - 14.1° . In the current elastic DCS measurements, instead, the missing angle ranges from $\theta_{\min} = 6.5^\circ$ to $\theta_{\min} = 16^\circ$. As expected, the missing angle is large at low energy and smaller at higher energies (Tables 6.3 and 6.4), and it is also significantly larger for the measurements performed with a beach compared to the no-beach case.

Table 6.3. Estimates of the missing angles at selected energies for the present total cross section measurements with $M = 1$.

Energy (eV)	Missing angle θ_{\min} ($^\circ$)
1	14.1
2	9.9
5	6.3
7	5.0
10	4.2
20	2.9
30	2.4
40	2.1
50	1.9
60	1.7

Table 6.4. Estimates of the missing angles, influencing the present elastic differential cross section measurements, are given at the investigated positron scattering energies together with the corresponding M value.

M	Energy (eV)	Missing angle θ_{\min} ($^\circ$)
1	1	16.0
1	2	11.3
1	5	7.1
1	6	6.5
5	8	13.4
5	10	12.4
5	15	9.7
5	20	8.1
5	25	7.3

In Section 2.2.3.3 we thoroughly examined the forward angle scattering effect that invariably affects all kinds of linear transmission based experiments, including the measurements presented here. There, we observed that the extent of this effect basically depends on the energy-dependent angular discrimination of the apparatus and on the nature of the absolute elastic DCS of the species in question in that angular range (see also Sullivan *et al.*, 2011). So, if these two quantities are known at all

scattering energies, then the total cross sections could be corrected, at least in principle, for the forward angle scattering effect.

In effect, as we have noted earlier, the angular discrimination as a function of the scattering energy and for a given M value can be calculated with Eq. (2.44). This is now actually known for the present experimental conditions from Table 6.3. Some elastic DCSs for the positron-THF system are also available as a part of the present thesis (see Section 6.3.2.5). Hence, the correction for the forward angle scattering effect could, in principle, be calculated by following the procedure described in Section 2.1.3.4. However, first, elastic DCS measurements for positron collisions with THF are unfortunately not available at all energies, since this would imply measuring the DCS at more than 80 different energies. Secondly, even if all these elastic DCSs were available, they would in any case be affected by the experimental missing angle, which in turn can be fairly large, as Table 6.4 clearly shows. Hence, the shape and magnitude of the DCSs is unknown in the range corresponding to the missing angle. This means that the forward angle scattering correction cannot be calculated, unless theoretical DCS results are available. Unfortunately, to the best of our knowledge, calculations of elastic DCSs for positron impact on THF are currently unavailable, so that this alternative is also not viable at this time.

The TCS results we report in the next section are, therefore, uncorrected for the forward angle scattering effect. As a consequence, these data represent a lower bound on the exact cross section values. We remind the reader that a thorough discussion of the angular discrimination issue and its effects on the measured cross sections can be found in Section 2.2.3.3. More specific information on this topic is also contained in the recent paper by Sullivan *et al.* (2011).

6.3.2 Results and discussion

The present total, positronium and elastic differential cross section for positron-THF scattering measurements are presented and discussed in the following subsections. The total cross sections are also compared with the only available earlier experimental results. These measurements have been undertaken for impact energies in the range ~ 1 -60 eV.

6.3.2.1 Total cross section

Our total cross section results for positron scattering from THF are plotted in Fig. 6.8 and listed in Table 6.5, as a function of the incident positron energy. Note that the error bars given in Table 6.5 and shown in Fig. 6.8 represent the statistical uncertainties on the TCS data only. The statistical errors amount to 0.5-3.2% ($\pm 1\sigma$), with the biggest errors being found at the highest energies. The overall errors are calculated as the square root of the quadratic sum of the individual contributing errors, like the statistical uncertainty, the uncertainty on the thermal transpiration correction and the uncertainty due to the drift of the Baratron zero. The absolute uncertainties are estimated to be in the range ~ 2 -12%, with the largest total errors again occurring at the higher energies (above 6 eV).

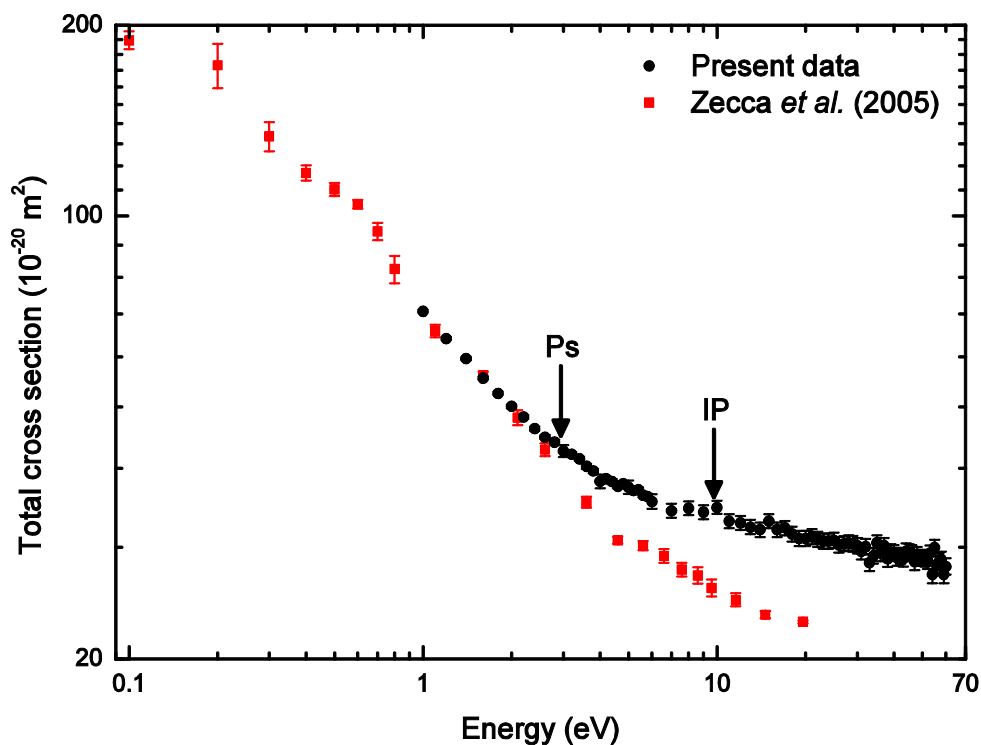


Fig. 6.8. The present total cross sections for positron scattering from tetrahydrofuran are compared with the only previous experimental results by Zecca *et al.* (2005). The thresholds corresponding to the positronium formation energy and the first ionisation potential are indicated by black arrows labelled “Ps” and “IP” respectively. Note that the error bars on the present cross sections and those on the data by Zecca *et al.* (2005) represent only the statistical uncertainties and are at the one standard deviation level.

Fig. 6.8 clearly shows that the present TCS decreases monotonically in magnitude as the positron energy increases, with an energy dependence that is very similar to a $\sim 1/\sqrt{E}$ function from the lowest energy up to the positronium formation threshold $P_s = 2.94$ eV (see Table 6.15). We believe that this behaviour and the magnitude of TCS in this energy range are due to the large permanent dipole moment $\mu = 1.63$ D (Bouchiha *et al.*, 2007) and dipole polarisability $\alpha = 47.08$ a.u. (see section 6.4.2) of the THF species. Both properties are, in fact, expected to play an important role in the positron-molecule interactions driving the scattering dynamics at these low energies. The effect of the opening of the positronium and then the direct ionisation scattering channels is apparent in Fig. 6.8, as a change in the TCS slope near the threshold energies corresponding to the positronium formation $P_s = 2.94$ eV and the first ionisation potential $IP = 9.74$ eV (Inoue *et al.*, 1993), respectively (see Table 6.15). As a result of these two inelastic channels becoming open, the TCS appears to be decreasing slowly in magnitude as the positron energy increases or even to be sitting essentially on a plateau, at least at the highest energies investigated in the present measurements.

Table 6.5. The present total cross sections for positron scattering from tetrahydrofuran, together with the statistical uncertainties on the data.

Energy (eV)	TCS (10^{-20} m^2)		Energy (eV)	TCS (10^{-20} m^2)	
	Average	Error		Average	Error
1.00	70.80	0.36	21.00	31.20	0.84
1.20	64.10	0.35	22.00	30.90	0.86
1.40	59.60	0.35	23.00	30.70	0.84
1.60	55.50	0.35	24.00	30.70	0.85
1.80	52.50	0.35	25.00	30.80	0.84
2.00	50.10	0.35	26.00	30.30	0.85
2.20	48.20	0.34	27.00	30.40	0.82
2.40	46.20	0.36	28.00	30.50	0.84
2.60	44.80	0.34	29.00	30.40	0.86
2.80	44.00	0.36	30.00	30.20	0.85
3.00	42.60	0.93	31.00	29.60	0.87
3.20	42.10	0.35	32.00	30.10	0.84
3.40	41.40	0.34	33.00	28.40	0.87
3.60	40.30	0.35	34.00	29.10	0.83
3.80	39.60	0.35	35.00	30.50	0.85
4.00	38.15	0.94	36.00	29.40	0.85
4.20	38.50	0.35	37.00	30.20	0.85
4.40	38.10	0.35	38.00	28.80	0.86
4.60	37.50	0.34	39.00	29.50	0.85
4.80	37.80	0.35	40.00	29.40	0.83
5.00	37.35	0.92	41.00	28.90	0.84
5.20	36.90	0.35	42.00	29.10	0.87
5.40	37.00	0.34	43.00	28.80	0.83
5.60	36.30	0.35	44.00	29.60	0.84
5.80	36.10	0.35	45.00	29.50	0.84
6.00	35.45	0.93	46.00	29.40	0.85
7.00	34.30	0.89	47.00	28.50	0.88
8.00	34.60	0.85	48.00	29.20	0.84
9.00	34.10	0.87	49.00	28.90	0.85
10.00	34.70	0.83	50.00	28.90	0.85
11.00	33.00	0.84	51.00	28.80	0.82
12.00	32.80	0.84	52.00	28.60	0.86
13.00	32.30	0.84	53.00	29.40	0.82
14.00	32.00	0.85	54.00	27.20	0.86
15.00	33.00	0.84	55.00	30.00	0.85
16.00	32.00	0.83	56.00	28.20	0.83
17.00	32.20	0.84	57.00	28.50	0.88
18.00	31.50	0.86	58.00	28.70	0.83
19.00	31.00	0.84	59.00	27.20	0.86
20.00	31.00	0.84	60.00	28.00	0.82

We have observed earlier that there are currently no calculations of the TCS for positron-THF collisions in the literature, while only one previous

experimental investigation at the TCS level on this species currently exists. This is due to Zecca *et al.* (2005) and was carried out with the positron spectrometer of University of Trento. Let us now compare our data with these earlier results in Fig. 6.8. We first note that, although the data by Zecca *et al.* (2005) are at a lower energy resolution (slightly less than 300 meV) compared to the present results (~44 meV during these specific TCS measurements), they go to lower energy (to 0.1 eV), whereas the present data stops at the lowest energy of 1 eV. We find a very good agreement between the present results and those by Zecca *et al.* (2005) in the common energy range between 1 eV and the positronium formation threshold. Above Ps, however, that agreement is no longer observed, with the Zecca *et al.* (2005) TCS being ~25% lower in magnitude than the present results at 20 eV. We believe that there are a few reasons that might explain the discrepancy we observe, in the magnitude of these two TCSs, at these high energies.

First of all, note that the error bars on the cross section shown in Fig. 6.8 represent the statistical component of the total uncertainty only. Zecca *et al.* (2005) estimate the absolute uncertainties on their data to be $\pm 3.5\%$ at the higher energies and $\pm 13\%$ at the lower energies, with the main contribution originating from the uncertainty in the pressure determinations. Thus, if we account for the overall uncertainties on the present cross sections and those of Zecca *et al.* (2005), then some of the discrepancy in Fig. 6.8 vanishes over parts of the common energies. The residual difference between the two TCSs might then be explained in terms of three other possible factors that can affect the TCSs in different ways.

First, even if the angular discriminations of the ANU and Trento apparatus are very similar they are not identical. In fact, we note that the angular discrimination affecting the present results (see Table 6.3) is slightly smaller than that characterizing the measurements carried out with the Trento apparatus (see Table 2.5). This implies that the present results should be somewhat higher in magnitude compared to the data by Zecca *et al.* (2005), because they would need a smaller correction to account for the forward angle scattering effect. This is exactly what we see in Fig. 6.8 at energies above the positronium formation threshold. Since the angular discrimination is energy dependent, this difference in the forward angle scattering correction could contribute somewhat to the observed discrepancy in the TCS magnitudes. Of course, this would also imply that the very good agreement, at the lower energies, that is currently observed would no longer be found. However, the uncertainties at the lower energies on the data of Zecca *et al.* (2005) (13%) would probably still lead to fair overall agreement, below Ps, between the two data sets.

Second, as we have seen at the beginning of Section 6.3, THF is known to possess three symmetric and two asymmetric conformers (Cadioli *et al.*, 1993). The relative amount of each of these conformers generally depends on the temperature and the pressure of the sample, so that if these parameters are changed for two individual THF samples, diverse conformational mixes might be in play. Different conformers may well have dissimilar physico-chemical properties, like the dipole polarisability or the

dipole moment (see e.g. 3H-THF in Section 6.4). As we have observed before, these two properties can have a big effect on the magnitude of the cross section, so that THF samples with different conformational mixes might show cross sections that are somewhat dissimilar in magnitude. Now, while the experiments at University of Trento and ANU were conducted at the same room temperature ($\sim 24 \pm 2$ °C), the typical pressures employed during the measurements may have not been the same. In effect, in the experiment by Zecca *et al.* (2005) the pressure in the scattering region was set such that the attenuation factor $A \geq 0.7$, while during the present measurements that pressure was regulated to allow for only $\sim 10\%$ of scattering events (i.e. $A \approx 0.9$). This difference might thus explain part of the observed discrepancy in the TCS magnitude of the two data sets. Nevertheless, the experimental dipole polarisabilities and dipole moments of the THF conformational isomers, except for the global minimum conformer, are, to the best of our knowledge, currently unknown, so that this hypothesis cannot be checked further at this time.

Third, the purity of the THF samples employed in the two experiments was also different. The sample used during the current measurements had a purity of 99.9%, while that in use at University of Trento had a purity $>99\%$ (Zecca *et al.*, 2005). Although this small difference is expected to have a minor, if not negligible, effect on the TCS, it might still contribute a little to the discrepancy observed between the TCS magnitude of the Trento (Zecca *et al.*, 2005) and the present measurements.

6.3.2.2 Positronium formation cross section

The present positronium formation cross sections for positron scattering off THF are listed in Table 6.6 and plotted in Fig. 6.9. The energy range investigated in this case was 1.2-60 eV. The errors given in Table 6.6 and shown in Fig. 6.9 are the statistical uncertainties on the measured data, estimated as one standard deviation of the average cross section at a given energy, and normally amount to 3-17% throughout the investigated energy range. The total uncertainties on the present results are generally in the 5-20% range, the smallest errors occurring at the lower energies. The statistical uncertainties thus represent the largest contribution to the overall errors.

Fig. 6.9 shows that our positronium formation cross section has the typical shape for a scattering channel stemming from a threshold-like process. The cross section below the known positronium formation threshold energy, $P_s = 2.94$ eV (see also Table 6.15), of THF (indicated by the red vertical line in Fig. 6.9) is essentially zero, as expected. Above that threshold the cross section dramatically increases in magnitude with increasing positron energy, until it reaches an absolute maximum around 15 eV. At this energy the ratio of the positronium formation to total cross section is also greatest. The positronium formation cross section starts decreasing in magnitude from about 15 eV and onwards, possibly as a result of the competition with the direct ionisation process becoming progressively stronger with increasing energy. Note that the direct ionisation channel opens at the first ionisation potential of THF, i.e. $IP = 9.74$ eV (Inoue *et al.*,

Table 6.6. The present positronium formation cross sections for positron scattering from tetrahydrofuran together with the statistical uncertainties.

Energy (eV)	Cross section (10^{-20} m^2)		Energy (eV)	Cross section (10^{-20} m^2)	
	Average	Error		Average	Error
1.20	0.14	0.28	22.00	10.80	0.62
1.40	0.36	0.27	23.00	10.30	0.59
1.60	-0.27	0.26	24.00	10.00	0.62
1.80	0.14	0.26	25.00	9.53	0.61
2.00	-0.13	0.27	26.00	10.10	0.61
2.20	0.08	0.26	27.00	9.40	0.60
2.40	-0.17	0.27	28.00	9.17	0.60
2.60	0.16	0.25	29.00	8.94	0.61
2.80	0.83	0.27	30.00	9.39	0.60
3.00	1.78	0.70	31.00	8.21	0.62
3.20	2.41	0.26	32.00	8.25	0.60
3.40	2.74	0.25	33.00	8.00	0.62
3.60	3.29	0.26	34.00	8.75	0.61
3.80	3.21	0.26	35.00	8.07	0.61
4.00	3.35	0.70	36.00	7.02	0.61
4.20	3.49	0.25	37.00	7.48	0.61
4.40	3.90	0.26	38.00	6.42	0.59
4.60	4.03	0.25	39.00	7.56	0.60
4.80	4.62	0.25	40.00	7.08	0.60
5.00	5.50	0.68	41.00	6.65	0.61
5.20	5.46	0.25	42.00	6.21	0.63
5.40	6.06	0.25	43.00	6.46	0.60
5.60	6.51	0.25	44.00	5.85	0.61
5.80	6.40	0.26	45.00	6.25	0.61
6.00	7.49	0.66	46.00	5.93	0.61
7.00	8.86	0.62	47.00	5.49	0.61
8.00	10.10	0.60	48.00	5.90	0.62
9.00	10.40	0.61	49.00	4.88	0.61
10.00	11.60	0.61	50.00	5.22	0.62
11.00	12.10	0.60	51.00	5.21	0.62
12.00	10.80	0.60	52.00	4.18	0.62
13.00	11.40	0.60	53.00	4.72	0.61
14.00	12.00	0.60	54.00	3.47	0.62
15.00	12.20	0.59	55.00	4.63	0.62
16.00	11.60	0.60	56.00	2.86	0.59
17.00	11.10	0.59	57.00	3.49	0.62
18.00	11.70	0.63	58.00	3.03	0.61
19.00	11.10	0.62	59.00	1.43	0.62
20.00	10.60	0.61	60.00	1.89	0.62
21.00	10.70	0.61			

1993) (see also Table 6.15). From the cross section trend highlighted in Fig. 6.9, at the highest energies investigated in the present measurements, we can

reasonably expect the positronium formation cross section for THF to tend to zero at about 70-80 eV incident energy.

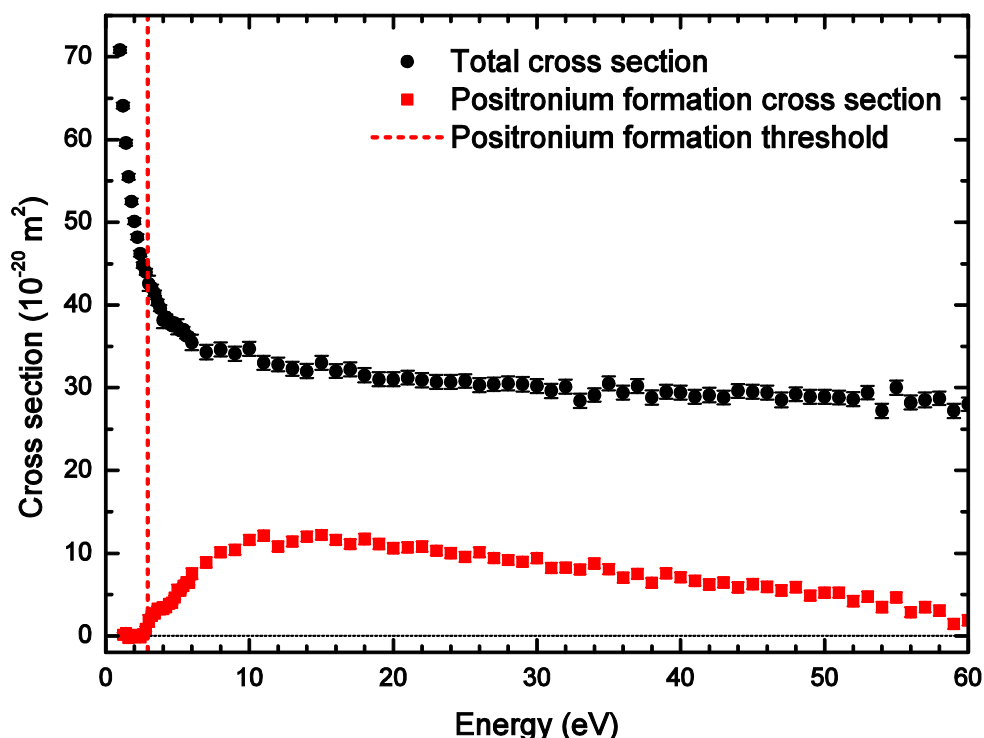


Fig. 6.9. The present total and positronium formation cross sections for positron impact on tetrahydrofuran. The error bars on the data represent the statistical uncertainties on the cross sections. The positronium formation threshold energy is indicated on the plot by the red dashed vertical line.

6.3.2.3 Inelastic scattering

Neglecting rotational and vibrational excitation, for the reasons described earlier, the scattering channels that contribute to inelastic scattering other than positronium formation are electronic excitation and direct ionisation. In THF the energy thresholds of the first electronic excited state 1B_1 is $E_{\text{exc}} = 6.57$ eV (Tam and Brion, 1974), while the first ionisation potential is $IP = 9.74$ (Inoue *et al.*, 1993). The successive electronic excitation states that THF is known to possess and the second, third, etc. ionisation potential of THF are reported in Tables 6.7 and 6.8, respectively.

As explained in Section 2.2.3.2.3, information about inelastic scattering can be obtained by directly measuring the integral cross section of the inelastic process of interest. However, the opening of the various inelastic channels can also be inferred simply from a long-range retarding potential analysis of the positron beam with the THF vapour in the cell and in the presence of a suitable beach (see again Section 2.2.3.2.3 and in particular Fig. 2.33). An example of such a long-range RPA2 cut-off curve, with THF vapour routed to the scattering region and a beach of $M = 5$, is shown in Fig. 6.10. In this case the transport energy was $E_{\text{tr}} = 50$ eV, while the retarding

potential analysis was carried out at a scattering energy $E_{sc} = 30$ eV. This means that the purely (if neglecting vibrations and rotations) elastic channel is constrained into a potential range ΔV of:

$$\Delta V = V_{sc}/M = 30 \text{ V}/5 = 6 \text{ V}, \quad (6.5)$$

Table 6.7. List of electronic transitions in THF and their corresponding experimental energy thresholds, as given by different references. Triplet states are not included in the table, because they cannot be excited by positrons with the THF ground state (1A_1) being a singlet (Bouchiha *et al.*, 2006). n_0 denotes the highest occupied molecular orbital (HOMO), $n_0 - 1$ indicates HOMO-1, the nl labels (3s, 3d, etc.) represent the Rydberg atomic orbitals and Ψ_l stands for the l th highest filled molecular orbital.

Transition (state)	Reference		
	Doucet <i>et al.</i> (1972)	Tam and Brion (1974)	Bremner <i>et al.</i> (1991)
$^1n_0 \rightarrow 3s$ (1B_1)	6.6	6.57	6.6
$^1n_0 \rightarrow 3p$	6.91	7.19	7.20
$^1n_0 \rightarrow 3p$			7.4-7.6
$^1n_0 \rightarrow 3d$	7.81		7.82
$^1n_0 \rightarrow 3d$		8.03	7.98
$^1n_0 - 1 \rightarrow 3s$			~8.1
$^1n_0 \rightarrow 4p$	8.30		8.57
$^1n_0 \rightarrow 5p$	8.73		8.89
$^1\Psi_3 \rightarrow 3s$		8.80	
$^1\Psi_3 \rightarrow 3p$		9.54	
$^1\Psi_7 \rightarrow 3s$		11.03	
$^1\Psi_8 \rightarrow 3s$		11.40	
$^1\Psi_{11} \rightarrow 3s$		13.61	

Table 6.8. List of experimental threshold energies for the ionisation potentials in THF (Tam and Brion, 1974).

Ionisation potential	Threshold energy (eV)
1st	9.73
2nd	11.51
3rd	12.02
4th	12.51
5th	12.97
6th	13.91
7th	14.19
8th	14.54
9th	15.35
10th	15.79
11th	16.84

down the RPA2 cut-off potential ($V_{co} = 50.175$ V in this case). The end of the region corresponding to the elastic scattering channel is highlighted by a black vertical bar in Fig. 6.10, and appears in the long range RPA2 cut-off curve as a step in the normalised amplitude of the positron pulse area. Above that threshold, the attenuation of the positron beam is entirely due to the inelastic processes like electronic excitations and direct ionisation. The energy threshold of the first electronic state 1B_1 ($E_{exc} = 6.57$ eV; Tam and Brion, 1974) and the first ionisation potential (IP = 9.74; Inoue *et al.*, 1993) in THF are indicated in Fig. 6.10 by a green and a blue vertical bar labelled “ 1B_1 ” and “IP”, respectively. The effect of the opening of the scattering channel corresponding to each of these two inelastic processes is clearly visible in Fig. 6.10, as a change in the slope of the RPA2 cut-off curve in the proximity of the respective energy thresholds.

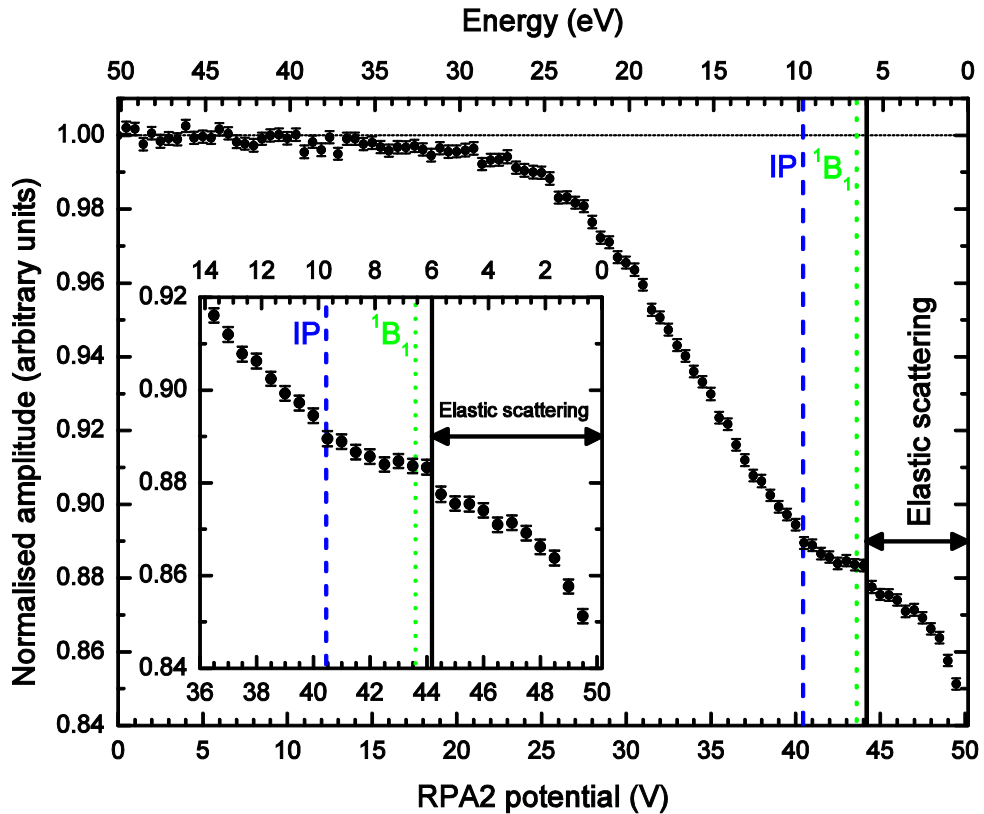


Fig. 6.10. Long range cut-off curve with tetrahydrofuran vapour in the scattering cell and with a beach ratio of $M = 5$. The normalised amplitude of the positron pulse area is shown as a function of the RPA2 potential (lower x -axis), or, equivalently, the positron incident energy (upper x -axis). The error bars represent the statistical uncertainties and are at the one standard deviation level. The end of the range corresponding to the elastic scattering channel, the threshold of the first excited state (1B_1) and the first ionisation potential (IP) are also indicated on the plot by black, green and blue vertical lines, respectively.

6.3.2.4 Elastic differential cross sections

The present results of the elastic differential cross section measurements, for positron impact on THF are reported in Table 6.9 and shown in Fig. 6.11, as a function of the elevation angle θ , and at the various investigated scattering energies. However, the DCS results are not given at all θ angles, but only in the range of acceptable angles $\theta_{\min} < \theta < \theta_{\max}$, where θ_{\min} is the missing angle (see Table 6.4 for the list of missing angles at each energy affecting the present elastic DCS measurements). In Table 6.9 and Fig. 6.11 the total uncertainties on our DCS data are also provided and these are typically in the range 6-38%. The statistical uncertainties amount here to 4-33%, indicating how large their contributions to the total errors are.

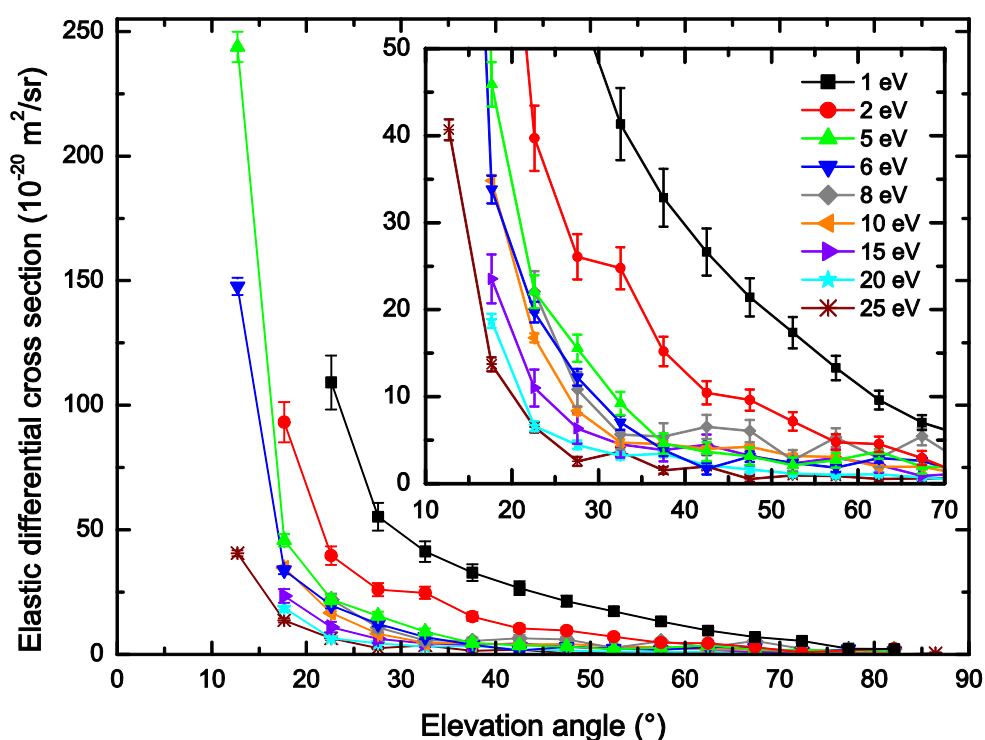


Fig. 6.11. The present elastic differential cross sections for positron scattering from tetrahydrofuran, at selected scattering energies. The error bars represent the total uncertainties on the cross sections.

Fig. 6.11 visibly illustrates that all the present DCSs dramatically decrease in magnitude as the elevation angle increases from the lowest angle towards 90° . But the most interesting aspect in Fig. 6.11 is how the present elastic DCSs become more and more peaked in the region of the most forward angles as the positron energy decreases. The predominantly forward peaked nature of the very low energy DCSs is particularly noticeable in Fig. 6.11, at scattering energies below 5 eV. We had anticipated this result, since this effect is thought to be largely due to the very polar nature of the THF species. In effect, we had already observed in the previous subsections the important role played by the large dipole moment and large dipole

polarisability of THF in enhancing the magnitude of the elastic ICS and the TCS towards lower positron energies. This earlier result is, therefore, perfectly consistent with the general picture we have drawn by comparing the DCS results shown in Fig. 6.11 at the various scattering energies.

Table 6.9. The present elastic differential cross section data for positron scattering from tetrahydrofuran, at selected scattering energies. The overall uncertainties on the cross sections are also given.

Angle (°)	E = 1 eV		E = 2 eV		E = 5 eV	
	DCS (10^{-20} m ² /sr)		DCS (10^{-20} m ² /sr)		DCS (10^{-20} m ² /sr)	
	Average	Error	Average	Error	Average	Error
12.73					243.91	6.10
17.66			93.26	8.05	45.91	2.55
22.61	109.23	10.82	39.72	3.74	22.06	1.89
27.58	55.34	5.54	26.08	2.62	15.57	1.56
32.55	41.34	4.16	24.78	2.42	9.20	1.34
37.53	32.88	3.32	15.20	1.69	4.62	1.17
42.51	26.63	2.71	10.44	1.33	3.67	1.08
47.49	21.42	2.20	9.61	1.22	3.13	0.99
52.47	17.36	1.80	7.15	1.06	2.11	0.91
57.45	13.29	1.42	4.77	0.90	2.69	0.85
62.42	9.59	1.08	4.54	0.87	3.70	0.82
67.39	7.02	0.85	2.95	0.79	1.93	0.77
72.35	5.49	0.73	0.95	0.73	1.91	0.76
77.27	2.38	0.53	1.62	0.74	1.47	0.74
82.10	2.18	0.54	2.35	0.76	1.75	0.75

Angle (°)	E = 6 eV		E = 8 eV		E = 10 eV	
	DCS (10^{-20} m ² /sr)		DCS (10^{-20} m ² /sr)		DCS (10^{-20} m ² /sr)	
	Average	Error	Average	Error	Average	Error
12.73	147.79	3.43				
17.66	33.82	1.59			34.82	0.65
22.61	19.72	1.18	22.06	2.39	16.75	0.52
27.58	12.24	0.96	10.84	1.98	8.35	0.43
32.55	7.00	0.82	5.66	1.71	4.71	0.37
37.53	3.87	0.71	5.40	1.53	4.55	0.33
42.51	1.69	0.65	6.53	1.39	3.99	0.30
47.49	3.10	0.60	6.04	1.28	4.23	0.27
52.47	2.39	0.55	2.66	1.19	3.19	0.25
57.45	1.83	0.51	5.29	1.09	3.07	0.24
62.42	2.93	0.49	2.92	1.06	1.94	0.23
67.39	2.63	0.48	5.43	1.02	1.93	0.22
72.35	1.11	0.45	2.29	1.01	1.01	0.21
77.27	2.07	0.46	0.31	0.97	0.42	0.21
82.10	1.47	0.47	2.26	0.99	0.69	0.22

Table 6.9. (continued).

Angle (°)	E = 15 eV		E = 20 eV		E = 25 eV	
	DCS (10^{-20} m ² /sr)		DCS (10^{-20} m ² /sr)		DCS (10^{-20} m ² /sr)	
	Average	Error	Average	Error	Average	Error
12.73					40.69	1.20
17.66	23.53	2.81	18.73	0.80	13.72	0.81
22.61	11.00	2.12	6.60	0.59	6.50	0.62
27.58	6.35	1.76	4.46	0.48	2.58	0.51
32.55	4.50	1.49	3.21	0.42	3.69	0.44
37.53	3.88	1.31	3.46	0.37	1.53	0.39
42.51	4.48	1.19	2.12	0.33	1.99	0.35
47.49	3.21	1.08	1.64	0.30	0.54	0.32
52.47	2.32	0.99	1.15	0.28	0.96	0.29
57.45	2.95	0.96	1.01	0.26	0.87	0.28
62.42	2.15	0.90	1.10	0.25	0.52	0.27
67.39	0.88	0.87	0.69	0.25	0.60	0.26
72.35	1.20	0.84	0.36	0.24	0.61	0.25
77.27	0.81	0.83	0.81	0.23	0.69	0.24
82.10			0.65	0.24	0.08	0.25
86.47					0.58	0.34

6.4 3-hydroxy-tetrahydrofuran

In this section we present the very first experimental results for positron impact on the important biomolecule 3-hydroxy-tetrahydrofuran. The TCSs for this species were collected with the positron spectrometer at the University of Trento.

3-hydroxy-tetrahydrofuran (3H-THF, C₄H₈O₂) is a heterocyclic ether similar to THF, except for the hydroxyl (–OH) functional group at position 3 on the five-atom ring (see Fig. 6.1). As we observed before, molecules such as tetrahydrofuran and 3-hydroxytetrahydrofuran are of interest to the community, because of their role as sugar rings in the backbone structure of the nucleic acids, so that they can be considered as prototypical building bricks for living matter (see Fig. 6.6).

Despite the experimental challenges that this molecule offers to conducting scattering measurements, owing to its “sticky” nature, 3H-THF has been recently investigated to some extent with electrons as a probe, with both experimental and theoretical absolute cross sections having been reported in the literature (Mozejko and Sanche, 2005; Milosavljević *et al.*, 2008; Vizcaino *et al.*, 2008). Unfortunately, collisions between positrons and 3H-THF have not been investigated to the same extent. Actually, to the best of our knowledge, there have been neither earlier measurements, nor calculations, for positron scattering from 3H-THF at all. As for THF, this lack of theoretical results may ensue from the difficulty in constructing a realistic enough physical model of the target, as well as of the interactions involved in the scattering process and in its different channels. As far as the measurements are concerned, the absence of data may, instead, well be due

to two technical issues. First, unlike THF (Zecca *et al.*, 2005), 3H-THF at room temperature is not particularly volatile (its vapour pressure is $P = 34$ Pa at a temperature of $25\text{ }^{\circ}\text{C}$; <http://www.chemspider.com/Chemical-Structure.9566.html?rid=06c0836d-3cb2-4cdc-b092-e85a3003d928>), thus making it rather challenging to generate enough gas vapour to achieve a sufficient attenuation of the positron beam intensity. Secondly, 3H-THF is known to be a mixture of at least two conformational forms with quite different physico-chemical properties, which might possibly complicate the interpretation of the experimental results. This circumstance, however, renders a comparison with the corresponding measurements for THF rather intriguing, the lowest conformer of THF having largely identical physico-chemical properties, as this enables us to infer some information on the role that the conformers of 3-hydroxy-tetrahydrofuran might play in the scattering dynamics.

6.4.1 Experimental details

The experiment on 3H-THF was conducted by following the directions described in Section 2.1, for scattering measurements using the positron spectrometer at the University of Trento. The target sample employed throughout these measurements was high-purity 3H-THF (99%, Aldrich). While 3H-THF is not a particularly volatile liquid, as noted above, pressures adequate to achieve a sufficient beam intensity attenuation were achieved during our measurements even at room temperature. However, the “sticky” nature of 3H-THF sometimes presented some experimental challenges in this respect. Our usual procedure in dealing with this problem was to immediately stop the data collection, and to simply let the system recover to the initial conditions, by pumping on the vacuum chamber until the next day. Once stable positron beam conditions had again been restored and the pressure in the scattering chamber had dropped back to the usual background vacuum, we resumed the measurements and started a new run.

The 3H-THF pressure inside the scattering cell ranged from 5 to 9×10^{-4} Torr and the pressure measurements were made with the 627B model Baratron operated at $45\text{ }^{\circ}\text{C}$. The thermal transpiration correction to the pressure readings, which is necessary because the target in the scattering region was at room temperature ($24 \pm 2\text{ }^{\circ}\text{C}$), was applied according to the instructions outlined in Section 2.1.3.2 and by assuming a molecular diameter for 3H-THF of 4.63 \AA . Note that this is the value we employed for the THF hard-sphere size, as given by Dampc *et al.* (2007b), since the molecular diameter of 3H-THF is currently unknown. This approximation is reasonable, given that the two molecules have a very similar structure and that computational chemistry simulations for various properties of the two species (see later) yield results in acceptable agreement with the experimental values. The thermal transpiration correction in this case enhances the measured TCS magnitude by less than 3% over the entire energy range.

The axial magnetic field present in the scattering region of the apparatus, to help focus the positron beam into the scattering cell, was held at a value

of $\sim 8\text{-}10$ G during the time of these measurements. This leads to a correction for the increased path length due to the gyration of the positrons in the magnetic field of $\sim 5\%$. Please note that, unlike in all other experiments that were performed with the Trento apparatus and are described in this thesis, the geometrical length L of the scattering cell in this case was noticeably longer, namely $L = 100.0 \pm 0.1$ mm, instead of $L = 22.1$ mm. Owing to the longer time that the positrons spent in the scattering region, the effective path length correction in this case is larger in absolute value, as compared with the other molecules investigated as a part of the present thesis.

The slow positron beam in this case was produced by the radioactive source (activity of ~ 3.8 mCi at the time of this experiment) in conjunction with a $1\ \mu\text{m}$ -thick tungsten moderator. A retarding potential analysis conducted as a part of the present experiment revealed that the energy resolution of the beam so obtained was ~ 0.3 eV (FWHM). We remind the reader that this finite energy beam width has a non-negligible effect on the magnitude of the TCSs, especially at the lowest energies (a few tenths of an eV), since the measured TCSs are convoluted over this energy resolution. As a result, the exact TCS is in reality a little higher in magnitude than what we measured at these very low energies (refer to Section 2.1.2.2 for more details on this effect). Note, however, that the extent of this effect depends on the actual shape of the TCS as a function of the energy.

6.4.2 Results and discussion

The present TCSs for positron scattering from 3-hydroxy-tetrahydrofuran are tabulated in Table 6.10 and plotted in Fig. 6.12 as a function of the positron energy, that in this case ranges from ~ 0.4 to 18.4 eV. In Table 6.10, together with the TCS values, we also provide the standard deviation of those TCSs, as an estimate of the statistical uncertainties affecting the present results at the various energies. These typically vary from nearly 3% to 7% over the range of different energies accessed in the present experiment, with an average uncertainty of $\sim 5\%$. As usual, the total errors on the present data (not given in Table 6.10) were estimated as the root of the quadratic sum of the single contributing errors, with the statistical uncertainties being the largest component of those errors. The overall uncertainties on the 3-hydroxy-tetrahydrofuran TCS measurements are found to span the $\sim 5\text{-}10\%$ range, and as usual the largest errors generally occur at the lowest energies.

Fig. 6.12 clearly shows a strong dependence of the TCS on the energy, with the TCS dramatically increasing with decreasing energy. We note that below the positronium formation threshold the TCS is characterised by a monotonic $\sim 1/E$ dependence on the positron energy E . This low energy TCS behaviour is very likely a consequence of the molecule having both a strong permanent dipole moment and an important dipole polarisability (see Table 6.11). These two properties are in fact the drivers of the dipole interaction and since for 3H-THF they are moderately large, the attractive polarisation potential between the incoming positron and the target molecule dominates

over the repulsive static mean field of the target nucleus in this low energy range. The overall potential is thus largely negative at these energies and so the probability of scattering between the projectile and the target is enhanced: this fact is reflected by the relatively higher values (compared to say THF) of the very low energy TCS that we observe in Fig. 6.12.

Table 6.10. The present total cross sections for positron scattering from 3-hydroxy-tetrahydrofuran. The statistical uncertainties are also given for each energy and are at the one standard deviation level.

Energy (eV)	TCS (10^{-20} m^2)		Energy (eV)	TCS (10^{-20} m^2)	
	Average	Error		Average	Error
0.41	193.04	14.10	5.00	25.53	0.81
0.50	170.77	6.45	5.40	27.60	1.49
0.60	148.69	6.58	5.90	27.32	2.48
0.70	132.49	12.00	6.40	26.01	1.88
0.80	120.57	7.43	6.70	27.22	1.51
0.90	101.12	3.91	7.00	25.58	1.77
1.00	86.09	3.05	7.40	25.03	0.52
1.10	79.29	4.55	7.70	24.77	1.91
1.20	76.88	3.33	8.00	24.28	1.57
1.30	70.06	3.72	8.40	25.35	0.48
1.40	70.79	4.79	8.70	24.80	0.55
1.50	66.80	4.00	8.90	22.24	1.91
1.60	62.81	2.76	9.40	23.42	1.71
2.00	45.91	0.76	9.80	22.82	1.24
2.40	43.83	1.71	10.40	21.99	1.13
2.90	37.20	1.91	12.40	19.95	0.46
3.40	34.78	2.10	14.40	19.10	0.76
4.00	29.63	1.24	16.40	18.31	1.14
4.40	29.52	0.95	18.40	19.55	0.95

Table 6.11. Present model chemistry (B3LYP/TZVP) results for the dipole moment (μ) and dipole polarisability (α) of THF and the two energetically most stable conformers of 3H-THF. The hard-sphere diameter (D) and the experimental dipole moment of THF are also given, along with the first ionisation potential (IP) and the positronium formation threshold (Ps) of the two species.

Property	THF	3H-THF	
		1 st conformer	2 nd conformer
D (Å)	4.63 ^a	≥ 4.63	≥ 4.63
μ (D)	1.96 exp. 1.63 ^b	1.74	2.88
α (a.u.)	47.08	50.68	50.98
IP (eV)	9.74 ^c	9.8 ^d	
Ps (eV)	2.94	3.0	

References: ^a Dampc *et al.* (2007b); ^b Bouchiha *et al.* (2007); ^c Inoue *et al.* (1993); ^d Giardini *et al.* (2005).

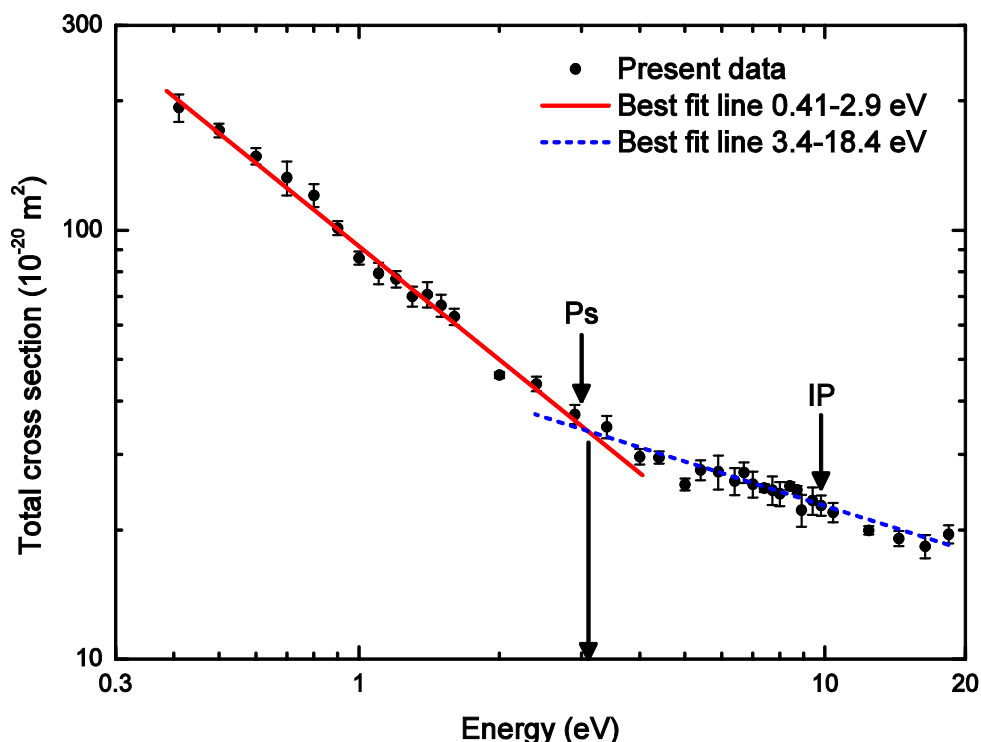


Fig. 6.12. The present total cross section results for positron scattering from 3-hydroxy-tetrahydrofuran as a function of the incident energy. The errors represent the statistical components ($\pm 1\sigma$) of the overall uncertainties. The arrows labelled “Ps” and “IP” indicate the positronium formation threshold and the first ionisation potential, respectively. Indicative best fit lines showing the change in slope of the TCS are also plotted. The vertical black arrow indicates the energy value where the two lines intersect.

In the present positron-3H-THF TCSs the effect of the opening of the positronium channel on the TCS is manifest as a change in the TCS slope at ~ 3 eV. In order to determine the positronium energy threshold from the present data, we have traced in Fig. 6.12 two best fit lines through the data, seeking to point out the energy where the monotonic decrease in the TCS changes slope as a result of the positronium channel becoming open. The lines are the least-squares fits to two subsets of the data, where the division between the points is set to maximise the ratio of the slope on the left to the slope on the right, with the condition that each subset must contain at least 10 points. We find that the first linear fit includes the points from 0.41 to 2.9 eV, while the second spans the energy range 3.4-18.4 eV and that these two lines intersect at about 3.1 ± 0.2 eV. Now, since the first ionization potential (IP) for 3H-THF is known to be 9.8 eV (Giardini *et al.*, 2005) and as the positronium threshold (Ps) can simply be obtained from the IP by employing Eq. 3.1, we find that $Ps = 3.0$ eV for 3H-THF (see Table 6.11). This value is consistent with the positronium formation threshold that we have determined above from the present TCS results, indicating that the opening of the positronium channel is very likely to be the cause of the change in the TCS behaviour observed around that energy.

As there are currently no other measurements, or any calculation of the cross sections, for positron collisions with 3H-THF that the present data might be compared to, we focus our attention on a comparison with the most similar species THF. In addition we try to see if the TCSs for these two molecules are related to the respective physico-chemical properties reported in Table 6.11. As we have seen in the previous section, there are two measurements of the TCS for the positron-THF system: one obtained as a part of the present thesis and the other one due to Zecca *et al.* (2005). Here we will limit the present discussion to a comparison of the present 3H-THF data with the results by Zecca *et al.* (2005), as both had been collected at room temperature with the same positron spectrometer at the University of Trento. Note that a discussion of the present THF TCSs as compared to the present 3H-THF results will be provided in the last section of this chapter, as part of a comparison between the data for all the biomolecules investigated in the present thesis.

In Fig. 6.13 we therefore compare the present 3H-THF TCSs with those for THF from Zecca *et al.* (2005). To better interpret the physics behind the TCSs behaviour shown in Fig. 6.13, we avail ourselves of some computational chemistry simulations with the software Gaussian (Frisch *et al.*, 2004), making use of the B3LYP/TZVP model chemistry. Note that we chose this model chemistry on the basis of its past ability to provide useful geometric and anisotropic parameters in biomolecules (Wang *et al.*, 2005; Jones *et al.*, 2006). The results of these calculations, for the dipole moment and dipole polarisability of THF (the two lowest energy conformers gave identical results) and of the two most energetically stable conformers of 3H-THF, are summarized in Table 6.11. First of all, we find that the present calculated value of the THF dipole moment ($\mu = 1.96$ D) is in quite good agreement with that determined experimentally ($\mu = 1.63$ D; Bouchiha *et al.*, 2007), a result which gives us further confidence in the efficacy of the B3LYP/TZVP model chemistry. It is also clear from Table 6.11 that the anisotropic parameters of both THF and the global minimum conformer of 3H-THF, are almost identical in value. Although not shown, the geometric values (i.e. bond lengths, bond angles) that we have calculated for these species are also very similar, suggesting that the hard-sphere size of these two molecules will be approximately equal. Under such circumstances we might reasonably expect the behaviour and magnitude of the TCSs for 3H-THF and THF to be also very similar below the positronium threshold. This is exactly what we see in Fig. 6.13 for energies E in the range $1.6 \leq E < 3.1$ eV. At even lower energies, however, the TCS of 3H-THF appears to be significantly larger in magnitude than that for THF. This effect may be due to the existence in our 3H-THF sample of the next most stable conformer of 3H-THF, which has a significantly larger permanent dipole moment compared to both that of its global minimum conformer and those of THF (see Table 6.11). As the dipole polarisabilities of THF and both 3H-THF conformers are almost identical to each other (again see Table 6.11), we believe that the TCS behaviour observed in Fig. 6.13, for positron energies below ~ 1.6 eV, is indicative of the presence of the second 3H-THF conformer with its bigger permanent dipole moment. The important role

played by conformers in the scattering dynamics is in essence not new, as this kind of conformational effect on molecular structure and activity has been appreciated in the physical chemistry community for quite some time now (Jones *et al.*, 2006).

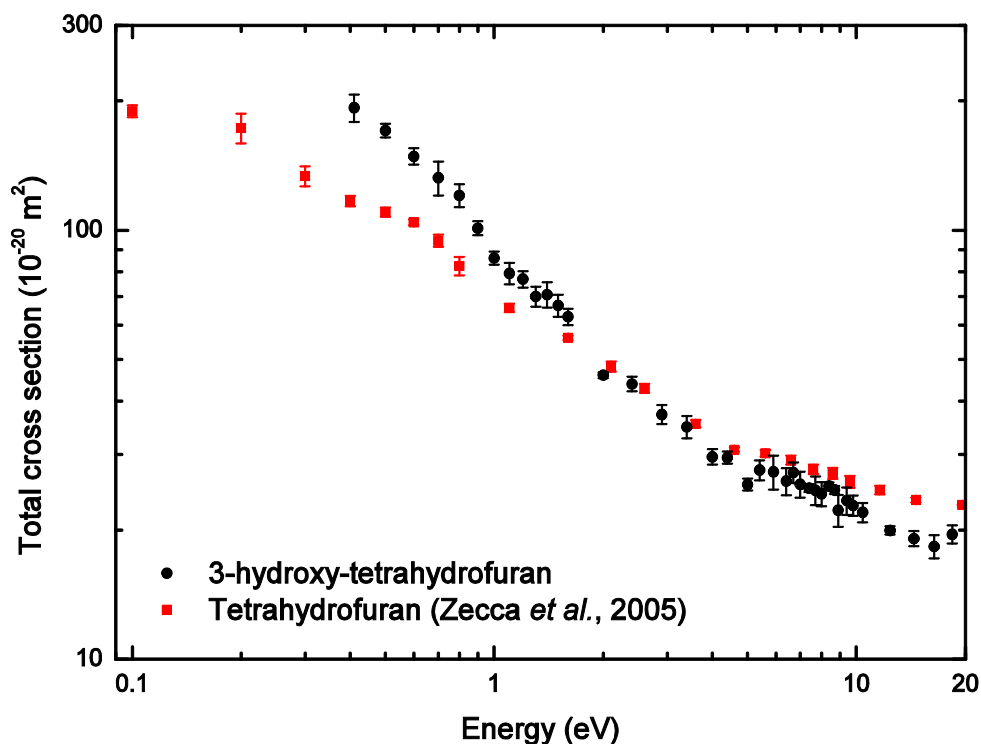


Fig. 6.13. The present total cross section results for positron scattering from 3-hydroxy-tetrahydrofuran are compared with the measurements on tetrahydrofuran performed by Zecca *et al.* (2005), with the same apparatus.

Notwithstanding the arguments we have presented above, a more accurate interpretation for the present 3H-THF TCSs can only be provided with the assistance of some guiding theory. As such calculations are currently lacking, theoretical consideration into this important biomolecule would be very welcome in the near future.

6.5 α -tetrahydrofurfuryl alcohol

In this section we introduce and discuss the original TCS results for positrons impacting on the α -tetrahydrofurfuryl alcohol biomolecule. Those data have again been measured with the Trento positron apparatus.

α -tetrahydrofurfuryl alcohol (THFA, C₅H₁₀O₂) is an aromatic compound belonging to a class of cyclic ethers, together with THF, 3H-THF and 3,4-dihydropyran (see Fig. 6.1). It has a five-member ring containing an ether group like THF, but with the α -hydrogen atom substituted by a -CH₂OH group. As shown in Fig. 6.14 and in the paper by Milosavljević *et al.*

(2006), the structure of THFA is very similar to that of 2-deoxy-D-ribose (deoxyribose, $C_5H_{10}O_4$), i.e. the pentanose monosaccharide contained in the DNA nucleotides, so that THFA can be considered a close analogue of that important biomolecule. This means that THFA is a very suitable model compound for investigating positron and electron collisions with biomolecules.

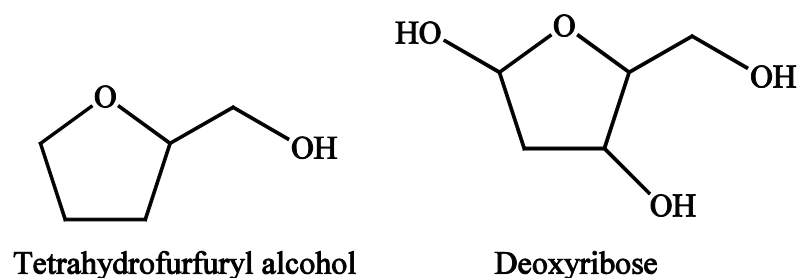


Fig. 6.14. Schematic drawings comparing the structures of the α -tetrahydrofurfuryl alcohol (THFA) and 2-deoxy-D-ribose (deoxyribose) molecules.

The particular physico-chemical properties that THFA is known to possess, render it also interesting to study from a fundamental perspective. THFA has a very large dipole polarisability $\alpha = 70.18$ a.u. (Szmytkowski and Ptasńska-Denga, 2011), which can be interpreted as the molecular electron charge cloud having quite a significant spatial extent. In addition, it has a relatively strong permanent dipole moment $\mu \sim 2$ D (Możejko *et al.*, 2006a). These two important properties are expected to have an important impact on the TCS behaviour, as we have seen in our previous investigations on polar molecules (see earlier chapters and previous sections of this chapter; see also Zecca *et al.*, 2011b) that such target molecular properties can have an important impact on the low-energy scattering dynamics. We note that this same kind of effect has also been observed for electron collisions with polar molecules (see e.g. Kato *et al.*, 2010a).

With regard to electron scattering from THFA, there are a few studies on the absolute cross sections for this species that had been investigated both from an experimental as well as a theoretical perspective. From the experimental side, we mention the total cross-section measurements by Możejko *et al.* (2006a), in the energy range 1-370 eV, and the elastic differential cross-section (DCS) results of Milosavljević *et al.* (2006), for energies from 40 to 300 eV and scattering angles of 30° - 110° . As far as concerns the calculations, some preliminary results based on the independent atom model (IAM) with screened additivity rule (SCAR) correction were reported in the same experimental-theoretical joint work by Milosavljević *et al.* (2006). More sophisticated theoretical results obtained with the same formalism, but this time satisfying the optical theorem and including rotational excitations, have been reported in another experimental-

theoretical joint study by Zecca *et al.* (2011a) together with the present TCS measurements.

Unfortunately, as far as we know, there have been no previous studies of positron scattering from THFA. The present data are, therefore, to the best of our knowledge, the first TCSs to be reported in the literature and as such, they fill an important void in our knowledge of the positron impact behaviour with that species.

6.5.1 Experimental details

The measurements on THFA were carried out according to the procedures outlined in Section 2.1, for scattering experiments conducted with the positron beamline in Trento. The target source used for this scattering experiment was a high-purity THFA sample (~99%), that we purchased from Sigma-Aldrich. Note that THFA is a liquid at room temperature and has a very low vapour pressure ($P = 186$ Pa at 25 °C; CERI, 2004) at room temperature. Nevertheless it is sufficiently volatile at that temperature to emit enough gas vapour, to achieve an adequate beam intensity attenuation in the scattering region, and allow us to carry out the measurements.

The pressure in the scattering region with THFA vapour routed to it ranged from 6×10^{-4} Torr to 1×10^{-3} Torr. As usual, a thermal transpiration correction was applied to the data, as the pressure in the scattering cell was measured by the 627B model Baratron operated at 45 °C, while the scattering cell was at room temperature (24 ± 2 °C). Note that the temperature of the THFA vapour was accurately measured by using a calibrated platinum (PT100) resistance thermometer in excellent thermal contact with the scattering chamber. In our geometry, gas molecules thermalise with the scattering cell walls and therefore the scattering chamber temperature can be considered as a good approximation of the gas temperature. Our sample holder was also thermally insulated in order to “damp down” the effect caused by any short-term room temperature fluctuations. The thermal transpiration correction was determined as described in Section 2.1.3.2, and by employing the molecular diameter of THF ($D = 4.63$ Å; Dampc *et al.*, 2007b) as that of THFA is unknown to us. This first-order approximation is justified by the observation that the THF molecule can be treated as a precursor to the structure of the THFA molecule, and that they are very analogous species (see Fig. 6.1). The correction on the TCS so calculated turned out to be typically $\sim +3\%$ in the entire energy range.

The positron path length L had to be corrected owing to the gyration of the projectile positrons in the scattering cell, caused by the axial magnetic field produced by the solenoid present in the scattering region (see Section 2.1.3.3). For incident positron energies in the range 0.15-30.15 eV, the intensity of the magnetic field was $B \sim 11$ G and so the value of L increased by $\sim 5.5\%$, whereas for energy values between 32.65 and 50.15 eV the intensity of the magnetic field was reduced to $B \sim 4$ G, leading to an increase in L of only $\sim 2\%$.

To produce our beam of slow positrons, we used a 1 μm -thick tungsten moderator in conjunction with the radioactive ^{22}Na isotope, whose activity was ~ 1.6 mCi during these measurements. For this experiment the retarding potential analysis revealed that the energy resolution of the beam was ~ 260 meV (FWHM), with an uncertainty on this determination of at most $\sim \pm 50$ meV. Note that this relatively low energy resolution was achieved thanks to an additional monochromation effect on the positron beam from the hemispherical deflector incorporated into the spectrometer design (see Section 2.1.2.1.1). We once again remind the reader that the TCS values we measured at the lowest energies are affected by the convolution of the real TCS with our energy beam width, meaning that the true TCSs are likely to be somewhat larger in magnitude than reported here.

6.5.2 Results and discussion

We present our positron-THFA TCS results as numerical data in Table 6.12 and in graphical form in Fig. 6.15, as a function of the incident positron energy. In this experiment the energy range where the TCS was investigated spanned 0.15-50.15 eV. The errors listed in Table 6.12 and plotted in Fig. 6.15, together with the corresponding TCSs, are purely statistical and are at the one standard deviation level. These are $\sim 5.5\%$ on average, although they vary from $\sim 3\%$ to $\sim 8\%$ for different energies. The overall uncertainty on our TCSs, estimated as the root of the quadratic sum of the single contributing errors, is not given in Table 6.12; however, we evaluated it to be within the 5-12% range. To help with the interpretation of the present results, in Fig. 6.15 we add two black arrows indicating, respectively, the approximate thresholds for positronium formation (Ps) and the first ionisation potential (IP) of THFA. The first IP of THFA is known to be 9.43 ± 0.12 eV (Milosavljević *et al.*, 2010), so from Eq. 3.1 we find a positronium formation threshold $\text{Ps} = 2.63$ eV for THFA.

In Fig. 6.15 the present data clearly shows a TCS energy dependence that resembles that of the other polar molecules examined in this thesis, that is to say, below the positronium formation threshold the TCS increases significantly in magnitude with decreasing energy. At the lowest energy (0.15 eV) the TCS reaches a very large magnitude, the highest ever encountered in all the investigations described in the present thesis. This magnitude is even more significant when we consider that the measured TCSs at the lowest energies are affected by the convolution effect over the finite energy resolution of the positron beam. In addition, the present TCSs are uncorrected for forward angle scattering effects (owing to the lack of positron-THFA elastic DCSs). These two factors, as the reader is by now very aware of, tend to cause an underestimation in the magnitude of the TCSs with respect to the real values, mostly at the lower energies (Makochekanwa *et al.*, 2009), so that when the TCSs are corrected for these effects they will somewhat further increase in magnitude. Note that, as THFA has a very large dipole polarisability and also a very large dipole moment, it is reasonable to assume that the elastic DCSs for positron scattering from THFA will be predominantly peaked at the forward angles, so that the forward scattering correction might be significant in this case.

Table 6.12. The present total cross sections for positron scattering from α -tetrahydrofurfuryl alcohol. The uncertainties represent the statistical components (one standard deviation) of the overall errors.

Energy (eV)	TCS (10^{-20} m^2)		Energy (eV)	TCS (10^{-20} m^2)	
	Average	Error		Average	Error
0.15	280.62	5.68	4.15	42.45	2.60
0.16	261.61	19.45	5.15	39.34	1.40
0.20	258.94	2.61	6.15	35.49	1.36
0.25	214.31	23.57	7.15	33.35	1.41
0.30	186.41	13.29	8.15	32.06	0.96
0.35	196.68	16.04	9.15	31.62	0.73
0.45	157.85	12.95	10.15	31.21	1.04
0.55	142.44	12.89	12.15	29.57	1.34
0.65	135.20	13.38	15.15	29.66	2.20
0.75	120.29	3.07	17.65	30.04	0.84
0.85	108.95	9.58	20.15	28.88	1.07
0.95	102.69	5.43	22.65	28.78	0.95
1.05	91.64	4.52	25.15	28.18	1.00
1.15	91.92	8.81	27.65	27.63	1.31
1.40	79.74	5.57	30.15	27.98	3.24
1.65	74.16	2.32	32.65	26.47	1.56
1.85	69.37	3.43	35.15	29.16	1.74
2.15	63.50	4.53	40.15	28.90	2.25
2.65	54.23	1.97	45.15	29.02	1.93
3.15	46.41	1.66	50.15	28.78	0.74

The low-energy behaviour of the present positron-THFA total cross-section was not unexpected, as we have encountered similar trends in analogous works on polar biomolecules (see previous chapters and the other sections in this chapter), which we have attributed to the strong dipole moments and significant dipole polarisabilities of those species. In this particular case the TCS shows a largely monotonic decrease in value with increasing positron energy up to the positronium formation threshold, with a slope that almost resembles a $\sim 1/\sqrt{E}$ function. Afterwards, when first the positronium, then the electronic excitation states and finally the direct ionisation channels successively open, their effect on the TCS is usually visible as a slope change and/or as a small bump in its distribution.

Since there are no other experimental or theoretical results for positrons impacting on THFA, in Fig. 6.15 we also plot the electron-THFA scattering results of the IAM-SCAR and IAM-SCAR + rotations computations, described in Zecca *et al.* (2011a), and the only electron impact TCS data on this species by Mozejko *et al.* (2006a). Let us first compare the experimental positron results (present TCSs) and the corresponding electron data of Mozejko *et al.* (2006a) (see Fig. 6.15). We find that the experimental results for the two leptons show a quite distinct behaviour, except perhaps above ~ 10 eV where both TCSs show roughly the same shape, although the electron TCS is almost twice as large in magnitude compared to that for the

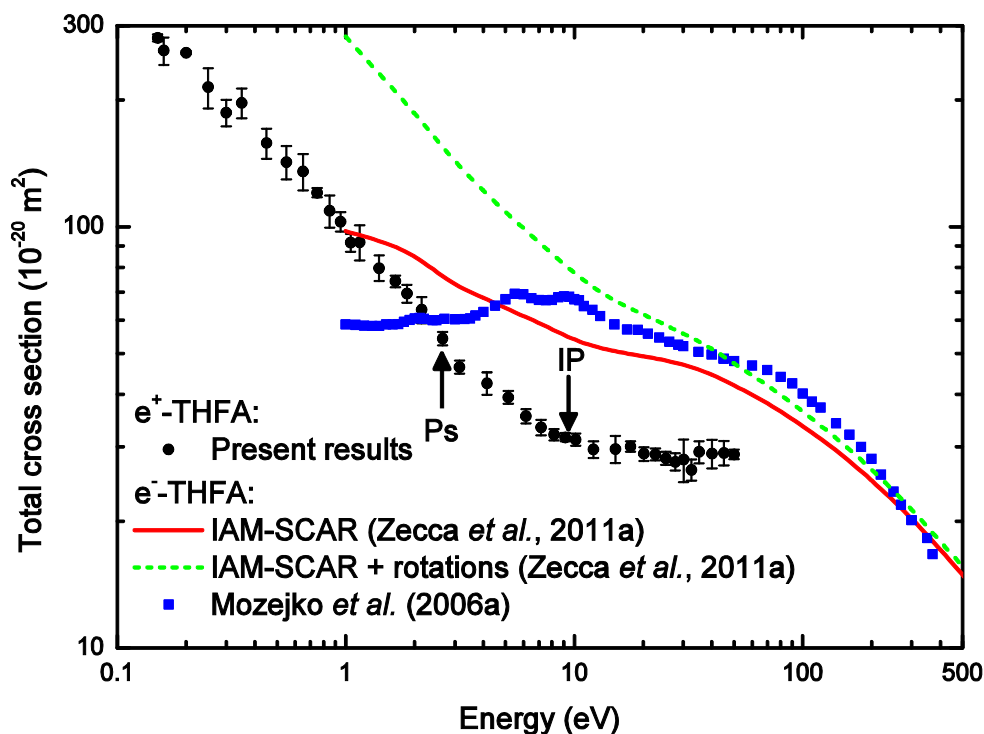


Fig. 6.15. The present total cross section results for positron scattering from α -tetrahydrofurfuryl alcohol are compared to theoretical electron scattering TCSs, within the IAM-SCAR and IAM-SCAR + rotations formalism by Zecca *et al.* (2011a), and the experimental electron TCSs from Mozejko *et al.* (2006a). The positronium formation threshold (Ps) and the first ionisation potential (IP) are indicated by black arrows.

positrons. The positron TCS is also largely featureless, displaying only the characteristic changes in slope at the opening of the Ps and IP thresholds, whereas the electron TCS displays a significant structure (showing up as two adjacent humps) associated with the temporary capture of the incident electron by the THFA molecule. In addition, the electron TCS keeps on increasing from the highest energy point down to 5.5 eV, where, quite surprisingly, it starts decreasing with decreasing energy until it meets the present positron TCS just above 2 eV. Thereafter it remains systematically lower in value as you go to still lower energies. We have just observed in the discussion above the very important role played by the target dipole moment and dipole polarisability in the low-energy positron scattering process. We would have expected also the electron TCS to increase significantly in magnitude with decreasing energy and, in any case, to increase more than the positron counterpart at the lower energies. The reason for the latter observation is that the two main forces (static and dipole interaction) driving the low-energy scattering dynamics are both attractive for electron collisions, as opposite to positrons, where only one of them (the polarisation potential) is attractive. In addition, in the electron channel the additional exchange interaction is also anticipated to contribute significantly to the interaction dynamics and thus to the value of the TCS. We therefore

believe that the fact the electron TCSs become lower in magnitude than the present positron TCSs below ~ 2 eV, might reflect a systematic limitation with the electron experiment. Possibly this might be associated with the Gdansk spectrometer having a relatively poorer angular discrimination compared to that of the Trento apparatus at the lower incident energies. Recall, in the context of our positron experiments, that we previously noted that the forward angle discrimination effect can significantly affect the TCS values at lower energies (see also Section 2.1.3.4). This same effect is also applicable to electron linear transmission TCS experiments, and as the data of Mozejko *et al.* (2006a) is not corrected for that effect, we believe that their lack of angular discrimination, at least in part, may cause their unexpected behaviour that we observe in Fig. 6.15 at the lower energies.

Comparing now the TCSs measured with positrons (present results) and those calculated for electrons by Zecca *et al.* (2011a) (again see Fig. 6.15), we observe that there is a qualitative correspondence (i.e. in shape) between them at lower energies. That is there is a similar energy dependence for both leptons, at least in the context of considering the IAM-SCAR + rotations formalism. As we would have expected in this case (see above), the theoretical electron TCSs turn out to be higher in magnitude than the corresponding positron data.

Finally, given the positron-THFA TCS trend shown in Fig. 6.15, at the higher energies, we estimate that the present positron TCS converges to the (either theoretical or experimental) electron TCS at an energy close to 200 eV. We believe this makes good physical sense, as contributions from the two most important phenomenological differences between the two leptons, positronium formation in the case of the incident positrons and exchange in the case of the incident electrons, both typically become small at incident projectile energies above 100 eV to 300 eV.

6.6 3,4-Dihydro-2H-pyran

In this section we report on the TCS measurements for positron scattering from 3,4-dihydropyran, a molecule that has also been experimentally studied with the Trento positron spectrometer.

3,4-dihydro-2H-pyran (C_5H_8O , DHP), equivalently known as 2,3-dihydro-4H-pyran, also belongs to the class of heterocyclic organic compounds known as cyclic ethers (i.e. containing an ether group of general formula R-O-R'), together with the other molecules THF, 3H-THF and THFA, that we have previously discussed (Fig. 6.1). Its structure is a six-atom ring, having five carbon atoms and one oxygen atom (see Fig. 6.1). DHP contains also one double bond between the two carbon atoms at position 5 and 6 (see Fig. 6.1). Again, like THF, 3H-THF and THFA, it possesses a sterically unhindered oxygen atom that carries two unshared pairs of electrons, which are expected to play an important role in the physico-chemical behaviour of the molecule. The main application of DHP is at protecting several chemicals, especially alcohols (Earl and Townsend, 1990; Kluge, 1990), but like all the other cyclic ethers of Fig. 6.1, it is also

used as an important solvent, as a chemical intermediate, or as the monomer for ring opening polymerisation.

We note that DHP possesses both a strong dipole polarisability ($\alpha = 64.92$ a.u.; <http://www.chemspider.com/Chemical-Structure.7789.htm>) and an important permanent dipole moment ($\mu = 1.38$ - 1.48 D; Soundararajan and Anantkrishnan, 1953; Scanlon *et al.*, 1995). As we have previously seen for our other highly polar targets, these two key properties will cause the scattering dynamics to be significantly influenced at the lower energies.

Despite the relevance of this molecule in biological processes, as pointed out by Nelson (2003), it appears this species has not been previously investigated from an experimental or a theoretical perspective, either with positrons or with electrons as a probe. Therefore, the present data are original.

6.6.1 Experimental details

As is our usual practice, we have followed the instructions described in Section 2.1 in order to perform the measurements with the positron apparatus at the University of Trento. A high-purity target DHP sample (>97%), provided by Aldrich, was used in the present measurements. Note that while the boiling temperature of di-hydropyran is fairly high (85-86 °C; <http://www.alfa.com/en/GP100W.pgm?DSSTK=L02731>), it is still volatile enough at room temperature (vapour pressure $P = 160$ hPa at 20 °C; Penn Specialty Chemicals Inc., 2004) to provide an appropriate source of gas vapour without any need for further heating.

In order to accurately measure the scattering cell pressure, which ranged between 7×10^{-4} Torr and 1×10^{-3} Torr, we used the 627B model capacitance manometer. We recall that the operating temperature of this device is 45 °C, so that a thermal transpiration correction needs to be applied to the measured pressures, since the target vapour in the scattering cell was at room temperature (25 ± 2 °C). As described in Section 2.1.3.2, an estimation of the hard-sphere diameter of the target molecule in question is needed in order to work out the thermal transpiration correction. Since the molecular size of DHP was unknown to us, we tried to predict its value by performing simulations with the software Gaussian (Frisch *et al.*, 2004) and with a B3LYP/6-31G model chemistry. These calculations generated a best estimate for the molecular diameter of 2.8 Å. We think that this result is likely to be underestimated, simply for the reason that a similar molecule THF, for instance, which has a five-atom ring, is known to be larger in size ($D = 4.63$ Å; Dampc *et al.*, 2007b). However, in the absence of an experimental value or higher level quantum chemistry value, we have chosen to employ this result. Hence the thermal transpiration correction turned out to be at worst $\sim +3\%$, on the magnitude of the TCS, over the entire energy range of this experiment.

To account for the path increase caused by the gyration of the positrons in the focusing axial magnetic field (~ 8 - 10 G in this case) present in the scattering region, we also corrected the value of L in the Beer-Lambert

equation (Eq. 2.13) to calculate the present TCSs. This correction was $\sim+5\%$ on L in this work.

A 1 μm -thick tungsten moderator was employed in conjunction with the radioactive source of ~ 2.4 mCi activity, at the time of these measurements, to produce the beam of slow positrons colliding with the target of interest. The moderated positron beam had an energy resolution of ~ 0.3 eV (FWHM), when calibrated with an RPA at the detection stage. This means that the measured TCSs are affected by the convolution over this finite energy beam width, indicating that the exact TCSs should somewhat increase in magnitude, particularly at the lowest energies, once corrected for this effect.

6.6.2 Results and discussion

In Table 6.13 and Fig. 6.16, we show the present TCS results for positron scattering off DHP. The measurements on this target were carried out at positron energies in between 0.15 eV and 48 eV. Note that the errors in Table 6.13 are simply the statistical uncertainties (estimated as one standard deviation) of the TCSs at each given energy, rather than the overall errors. The statistical errors are typically in the range 1-7% and amount to 4% on average over the energy range considered. The absolute errors on the TCSs are instead usually within the range 5-12%.

Table 6.13. The present total cross sections for positron scattering from dihydropyran together with the statistical uncertainty components ($\pm 1\sigma$) of the overall errors.

Energy (eV)	TCS (10^{-20} m^2)		Energy (eV)	TCS (10^{-20} m^2)	
	Average	Error		Average	Error
0.15	145.98	11.42	6.75	39.61	2.34
0.20	142.46	7.57	9.75	31.78	1.44
0.25	120.70	11.72	11.75	32.75	1.66
0.30	117.53	8.89	13.75	30.08	1.21
0.35	109.39	1.97	15.75	32.56	2.16
0.40	119.65	12.54	17.75	32.22	0.86
0.45	116.00	9.90	19.75	30.05	1.59
0.50	116.69	4.44	25.75	30.57	1.12
0.55	115.10	1.80	28.00	29.84	0.78
0.65	97.32	1.64	30.00	27.09	0.05
0.75	91.06	4.77	32.00	29.11	0.66
1.00	79.91	4.87	34.00	27.10	0.18
1.25	72.17	2.49	36.00	26.41	0.94
1.45	70.65	3.18	38.00	26.18	0.35
1.50	69.28	2.61	40.00	27.51	0.20
2.00	57.81	0.24	42.00	26.66	1.53
2.75	54.36	7.69	44.00	26.53	0.33
3.00	43.51	3.33	46.00	25.77	1.19
4.00	42.63	0.38	48.00	26.01	0.63
4.75	43.30	0.84			

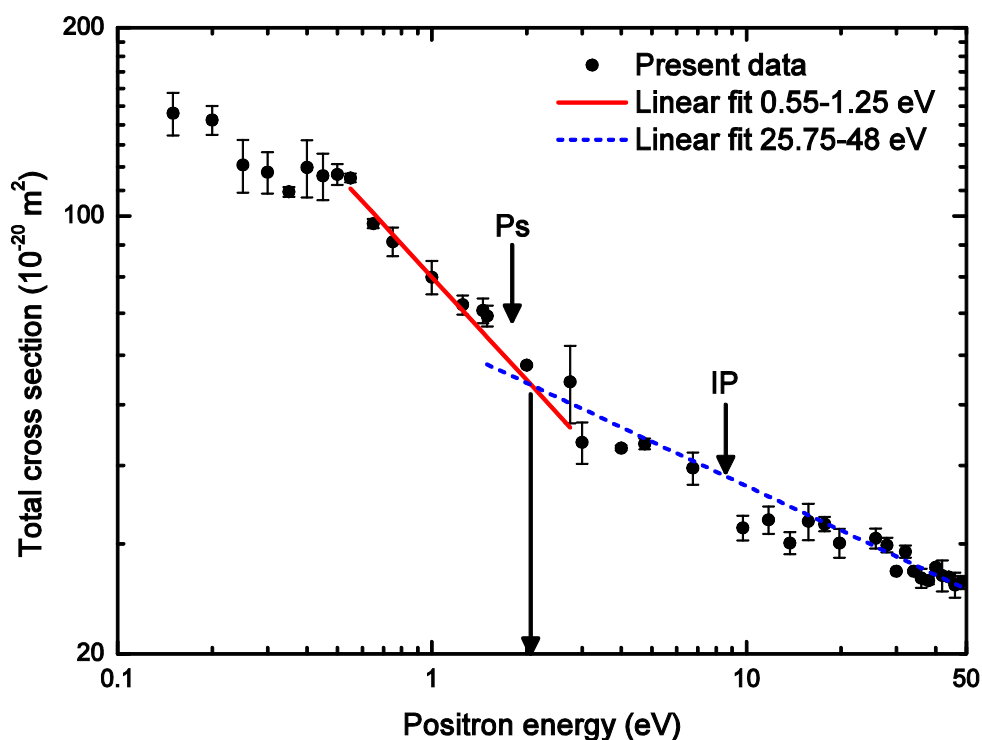


Fig. 6.16. The present total cross section results for positron scattering from di-hydropyran. The errors represent the statistical uncertainties (one standard deviation) only. The positronium formation threshold (Ps) and the first ionisation potential (IP) are indicated by black arrows. Least-squares linear fits to the two subsets of points in the energy range 0.55-1.25 eV and 25.75-48 eV are also plotted in order to show the change in the TCS slope. The vertical black arrow highlights the energy value at the intersection between the two best fit lines.

Fig. 6.16 clearly shows how the TCS considerably rises in magnitude for decreasing energies. This trend appears in Fig. 6.16 as a monotonic increase with a slope that can be traced back to a $\sim 1/\sqrt{E}$ energy dependence for energies approximately between the positronium formation threshold and ~ 0.5 eV. This TCS behaviour is consistent with what one would expect from a molecule like DHP, that has both a prominent dipole moment ($\mu \sim 1.38$ - 1.48 D; Soundararajan and Anantakrishnan, 1953; Scanlon *et al.*, 1995) and also a large dipole polarisability ($\alpha = 64.92$ a.u.; <http://www.chemspider.com/Chemical-Structure.7789.htm>). That is why the present DHP TCS below the positronium formation threshold appears to be very similar in shape to what we have previously seen in our investigations on other highly polar molecules (see, for instance, the previous sections in this chapter). Note also that, as a result of the simulations on the DHP structure that we have performed (see above), we were able to check for the veracity of these two important properties. Those calculations returned 1.70 D for the dipole moment and 58.89 a.u. for the dipole polarisability, values that turn out to be in quite fair agreement with the earlier data (Soundararajan and Anantakrishnan, 1953; Scanlon *et al.*, 1995;

<http://www.chemspider.com/Chemical-Structure.7789.htm>). We note that the rate of increase in the TCS seems to start diminishing with decreasing energy below about 0.5 eV. This observation may simply reflect the convolution effect of our finite energy resolution on the measured TCSs at these very low energies in this case.

It is manifest from Fig. 6.16 that the opening of the positronium channel, and possibly also that of direct ionisation, have an important effect on the magnitude of the TCSs above the respective threshold energies. As before, this essentially appears as a change in the TCS slope. In order to determine the positronium formation threshold from the present TCS data, we have drawn on the plot in Fig. 6.16 two lines of best fit, which seek to highlight at about what energy the monotonic decrease in the TCS with energy changes slope. To this end we have chosen two subsets of the data, such as to maximise the ratio of the slope of the line that fits the low-energy subset to that of the line fitting the high-energy subset. Note that the very low energy points (<0.5 eV), which are likely to be affected by the convolution caused by our finite energy resolution, are excluded from this analysis. We find that the first subset must include the points in the energy range 0.55-1.25 eV, while the high-energy one contains the data from 25.75 eV to 48 eV. As a consequence the two best fit lines intersect at about 2.1 ± 0.6 eV, where the rather large uncertainty here simply reflects the sensitivity of this determination to the choice of points included in the analysis. We have found two values for the first ionisation potential (IP) of DHP in the literature. The most recent one was reported by Stone and Lin (1980), who gave a value of 8.34 eV. This work is, however, at a lower resolution than that of Planckaert *et al.* (1974), who instead found a vibrational series of peaks in the range 8.35-8.85 eV for ionisation from the highest occupied molecular orbital of DHP. Taking the centroid value of those peaks as a reasonable estimate for the first ionisation potential, we obtain $IP = 8.60 \pm 0.25$ eV. As, for a given species, the positronium threshold energy (Ps) differs from the first ionisation potential (IP) by an amount equal to the positronium binding energy (Surko *et al.*, 2005) (Eq. 3.1), we find that $Ps = 1.80 \pm 0.25$ eV for DHP. This value is consistent with that for the positronium threshold that we have determined in Fig. 6.16, starting from our data, so that the energy where the TCS changes slope is again likely to be indicative for the positronium channel becoming open.

6.7 Pyrimidine

The first TCS measurements for positron scattering from our last important biomolecule, the nucleobase precursor pyrimidine, are introduced and discussed in this section. The results described in the following were carried out with the positron apparatus at the University of Trento.

Pyrimidine ($C_4H_4N_2$) is an aromatic compound containing two nitrogen atoms at positions 1 and 3 of a six-member ring (see Fig. 6.1). Pyrimidine represents the sixth and last species we investigated in the series of biologically relevant molecules schematically shown in Fig. 6.1. Note that

this series is not a homologous series, but it is clear from Fig. 6.1 that, except for formic acid, all the molecules are structurally related to a high degree.

The structure of the pyrimidine molecule is very similar to that of the three nucleobases cytosine, uracil and thymine (see Fig. 6.17). These three molecules build some of the nucleotides, i.e. the component units of the nucleic acids, and can all be considered as pyrimidine derivatives. They are all indeed called pyrimidine-bases, opposite to adenine and guanine that are purine-bases (i.e. stem from the purine molecule). Hence, due to this similarity, pyrimidine is also considered a model compound to investigate positron and electron collisions with the constituents of the nucleic acids (Levesque *et al.*, 2005).

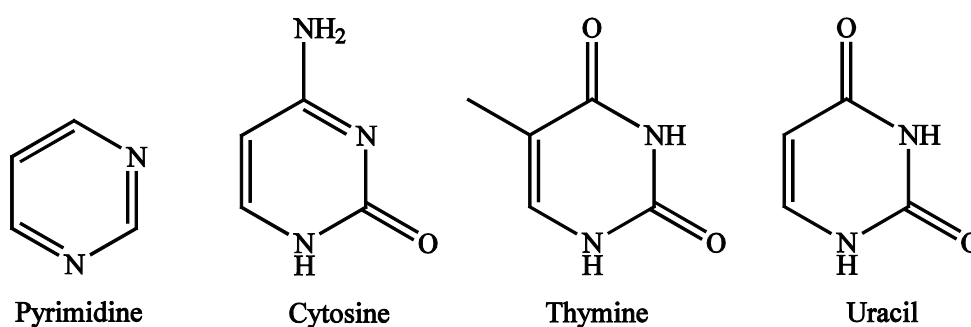


Fig. 6.17. Schematic diagram comparing the structure of pyrimidine with that of the pyrimidine-derived nucleobases cytosine, thymine and uracil, which are found in the nucleic acids.

Pyrimidine is not only an interesting molecule because of the crucial role it plays in biological processes, it also possesses several physico-chemical properties that make it worth examining from a fundamental perspective. Other than being considerably large in size (molecular diameter $D = 5.5 \text{ \AA}$; Spears and El-Manguch, 1977) and having a fairly big dipole polarisability $\alpha \sim 59$ ($\alpha_{xx} \sim 69$ a.u.; $\alpha_{yy} \sim 71$ a.u.; $\alpha_{zz} \sim 38$ a.u.; Hattig *et al.*, 1998; Jansik *et al.*, 2004), which implies its electron charge cloud has a quite significant spatial extent, pyrimidine also possesses a strong permanent dipole moment $\mu = 2.28\text{-}2.39$ D (Blackman *et al.*, 1970; Chen and Holroyd, 1996; Kisiel *et al.*, 1999). As we have previously seen in our positron scattering results, but this applies to electron scattering investigations as well (see e.g. the recent studies by Fuss *et al.*, 2009 and Kato *et al.*, 2010a), such target molecular properties can have an important influence on the scattering dynamics of the system under study, particularly at the lower impact energies.

Since, to the best of our knowledge, there have been no previous studies, either theoretical or experimental, of positron scattering from pyrimidine, so that the present data are the first TCSs to be reported, they fill an important void in the literature in our knowledge of molecular positron collisions. If we look, however, for electron scattering studies from this same species, we find that the situation is slightly better. In this respect we note the older

work by Palmer *et al.* (1990), who investigated the electronic excitation states of pyrimidine, both from an experimental perspective, through VUV absorption and near-threshold electron energy loss spectra, and a theoretical point of view, with *ab initio* multi-reference configuration calculations. Subsequently, vibrational and electronic-state excitations of pyrimidine condensed on a thin film of solid argon at 18 K were investigated by Levesque *et al.* (2005) for incident electron energies in the range 2-12 eV; nevertheless, these data were not collected on an absolute level. More recently, the first absolute elastic DCS measurements for electrons impacting with energy spanning 50-300 eV were published in a paper by Maljković *et al.* (2009). In this same paper they also reported some calculations from the independent atom-screened additivity rule (IAM-SCAR) method, and found good agreement between their experimental and theoretical results. A very recent elastic DCS and ICS study, for energies in the range 3-50 eV, was reported by Palihawadana *et al.* (2011). This study also included corresponding theoretical results. Note that we know of no experimental study reporting on TCSs for electron-pyrimidine scattering. From a theoretical perspective, instead, we note the only electron impact TCS calculation, within the independent atom-screened additivity rule (IAM-SCAR) formalism, performed by the ATMOP research group based in Madrid. This work was for the extensive energy range of 1-10,000 eV. These results have been published together with the present measurements for positrons in an experimental-theoretical joint paper, by Zecca *et al.* (2010c).

6.7.1 Experimental details

The experimental details and measurement techniques reported in Section 2.1, for the Trento spectrometer, comprehensively explain how the present experiments on pyrimidine have been carried out. Thus we need to provide here only some details in relation to this particular experiment.

A sample of highly pure pyrimidine (~99%) was purchased from Aldrich and was used for these measurements. Pyrimidine presents itself as a rather “oily” liquid at room temperature; nevertheless it turned out to be sufficiently volatile at that temperature, to let us perform our positron measurements on the gas phase molecules.

The scattering cell pressure was measured by using the standard 627B model capacitance manometer, which operates at a temperature of 45 °C, and ranged from 6×10^{-4} Torr to 1×10^{-3} Torr. The pressure readings need to be corrected for the thermal transpiration effect, since the target molecules in the scattering region were approximately at room temperature (24 ± 2 °C), that is accurately measured by a calibrated platinum (PT100) resistance thermometer in excellent thermal contact with the scattering chamber. This is again considered to give a good indication of the temperature of the pyrimidine vapour, which is in thermal equilibrium with the scattering cell walls. We used $D = 5.5$ Å (Spears and El-Manguch, 1977) as the best estimate of the molecular hard-sphere diameter of pyrimidine, in order to compute the thermal transpiration correction (Eq. 2.15). This

correction was at most +3.2% in the magnitude of the TCS, throughout the range of energies investigated in this experiment.

The intensity of the magnetic field, generated by the solenoid in the scattering region, was $B \sim 12$ G for the measurements at the lower energies up to 28.15 eV, while it was reduced to $B \sim 3$ G for those between 30 eV and 45 eV. To account for the path increase caused by the gyration of the positrons in the focussing axial magnetic field, the value of L was thus increased by $\sim 6\%$ and $\sim 1.6\%$, respectively.

A 1 μm thick tungsten moderator was used to moderate the positrons emitted by the radioactive source, with the activity of the isotope being ~ 1.7 mCi when these measurements were performed. The retarding potential analysis carried out with this moderator, just before this experiment was started, indicated that the energy width of the positron beam was ~ 260 meV, with an uncertainty on this estimate no greater than ± 100 meV. The convolution of the real TCS with this finite energy resolution implies that the measured TCS are somewhat underestimated in magnitude, especially at the lowest energies, where this effect is expected to be largest.

6.7.2 Results and discussion

The present TCS results for positron collisions with pyrimidine are given in Table 6.14 and are plotted in Fig. 6.18. The energy range of these measurements is 0.3-45 eV. Note that as usual the errors listed in Table 6.14 and plotted in Fig. 6.18 are purely statistical and are at the ± 1 standard deviation level. These are in the range ~ 2 -13% and amount to almost 8% on average. The overall errors, being estimated as the square root of the quadratic sum of each contributing error, the statistical uncertainty being only one of them, typically lie in the range 5-15% for the energies examined in this work.

In Fig. 6.18 the approximate thresholds for positronium formation (Ps) and the first ionisation potential (IP) of pyrimidine are indicated by a black arrow in each case. The first ionisation potential of pyrimidine lies in the range 9.33-9.73 eV (Bergmann, 1969; Buff and Dannacher, 1984; Dewar and Worley, 1969; Piancastelli *et al.*, 1983; Potts *et al.*, 2003), while we can estimate the positronium threshold by using the general formula of Eq. (3.1). On doing so, we obtain a corresponding range for Ps of 2.53-2.93 eV.

Once again, like for the other polar molecules investigated in this thesis, the TCS results obtained for pyrimidine (Fig. 6.18) clearly show that the TCS increases significantly in magnitude towards the lower energies. This magnitude would be even bigger than what the present results show, if they were corrected for the effects due to the convolution over the energy resolution of the positron beam and due to forward angle scattering. These two instrumental effects, in fact, affect the measured data in the whole energy range, although they have a much larger impact at the lowest energies (Makochekanwa *et al.*, 2009; Sullivan, 2011). Note that pyrimidine has a relatively huge dipole moment, so it is reasonable to assume that the forward angle scattering effect in pyrimidine might be more significant than

Table 6.14. The present total cross sections for positron scattering from pyrimidine. The error bars represent the statistical uncertainties only, and are at the one standard deviation level.

Energy (eV)	TCS (10^{-20} m^2)		Energy (eV)	TCS (10^{-20} m^2)	
	Average	Error		Average	Error
0.30	131.71	5.34	9.30	25.15	1.72
0.40	125.81	4.63	10.30	25.99	2.37
0.50	113.19	15.37	11.30	24.37	1.21
0.60	113.01	10.74	13.30	23.40	1.48
0.70	100.42	3.03	15.30	22.98	1.75
0.80	98.56	0.01	17.30	21.40	1.20
1.00	79.31	4.18	18.30	23.85	1.09
1.25	76.54	5.14	20.30	24.23	1.11
1.50	65.05	9.03	23.30	23.71	1.42
1.70	54.07	7.05	25.15	26.18	2.99
2.00	51.75	9.48	28.15	24.03	2.82
2.35	53.11	6.21	30.00	26.01	2.51
3.15	44.33	4.02	33.00	25.01	2.61
4.55	32.59	5.47	35.00	24.58	0.74
5.55	31.54	7.74	37.00	26.93	0.01
7.05	30.51	3.15	40.00	22.79	0.01
7.80	28.24	0.97	43.00	22.59	0.01
8.30	27.00	1.62	45.00	22.95	0.01

for the other less polar molecules, e.g. water and formic acid (see Makochekanwa *et al.*, 2009). The low-energy behaviour of the present positron-pyrimidine TCS is consistent with what we would have expected from a highly polar molecule, as we have detected similar trends in our previous studies on them throughout this thesis. Like in this case, the strong dipole moments and the significant dipole polarisabilities of these species are likely to be the reason for observing such a TCS shape. The TCS of pyrimidine essentially shows a largely monotonic decrease in value, as a function of the energy, with a slope that is close to $\sim 1/\sqrt{E}$ (see Fig. 6.18), until first the positronium channel, then the electronic-state channels (Palmer *et al.*, 1990) and finally the direct ionisation channel successively open. As before, the opening of these channels is usually seen as a small “bump” or a change in the slope of the measured TCS (again, see Fig. 6.18).

Since there have been no other investigations into positron collisions with pyrimidine, in Fig. 6.18 we compare the present positron TCS data with the corresponding electron impact results. As we have observed earlier, the only available electron work on pyrimidine at the absolute TCS level was reported by Zecca *et al.* (2010c). In that study electron TCS results were obtained by means of computations with the IAM-SCAR and IAM-SCAR + rotations formalism. In Fig. 6.18 we note the very large electron scattering cross sections for this species, which again indicate the very important role played by the target dipole moment in the low-energy electron scattering dynamics. By comparing our measured TCSs for

positrons and the calculated TCSs for electrons, we observe that there is a good qualitative (i.e. in shape) correspondence at the lower energies, at least with the IAM-SCAR + rotations method. Namely, we observe that there is a similar energy dependence for both leptons. As far as the magnitude of the TCS is concerned, the electron results are higher at these low energies, compared to the corresponding positron results, hence confirming our expectations based on the different nature of the interactions involved with these two particles of opposite electrical charge. This positron-electron correspondence in the TCS would probably become even more transparent, if the forward angle scattering corrections were to be applied to the measured positron data. At higher energies the present positron TCSs seem to trend towards the calculated electron TCSs, perhaps converging at around 200 eV. This is again consistent with our knowledge of the physics behind their scattering phenomena: it is well known that the two most important phenomenological differences between the two leptons, exchange in the case of the incident electrons and positronium formation in the case of the incident positrons, both typically become small at incident projectile energies above about 100 eV to 300 eV (Surko *et al.*, 2005).

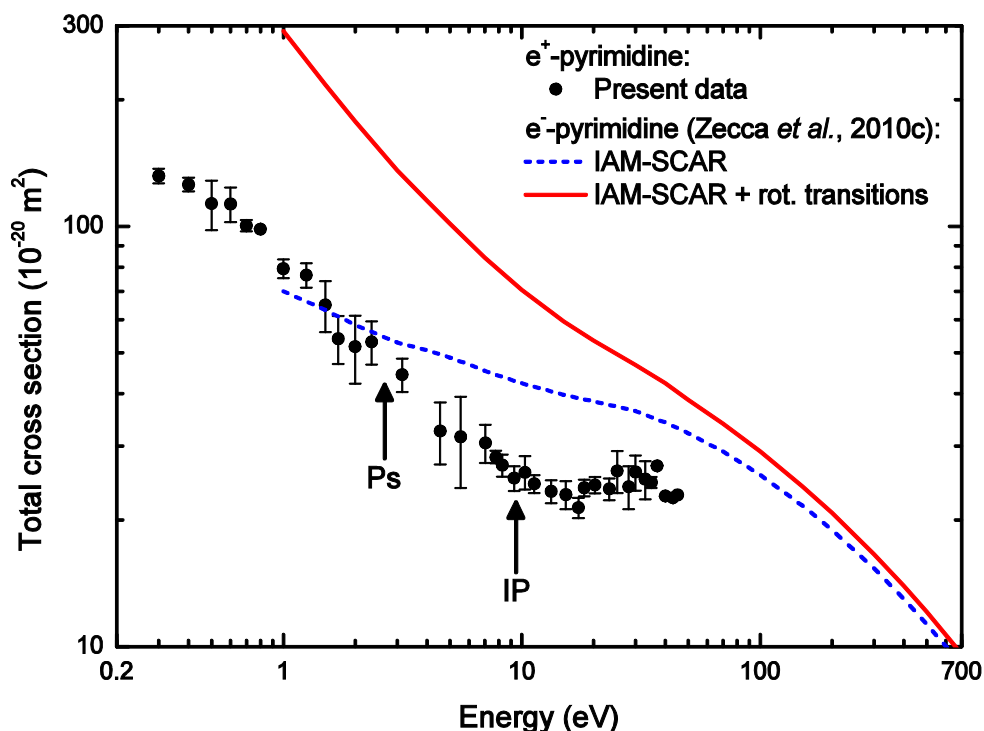


Fig. 6.18. The present total cross section results for positron scattering from pyrimidine. The errors represent the statistical components (one standard deviation) of the overall uncertainties only. The positronium formation threshold (Ps) and the first ionisation potential (IP) are indicated by arrows. Also plot are the TCS calculations for electron scattering within the IAM-SCAR and IAM-SCAR + rotations formalism by Zecca *et al.* (2011c).

6.8 Comparison between the molecules of biological interest

In Fig. 6.19 we compare the TCSs from all the six biomolecules shown in Fig. 6.1, which have been studied as a part of the present thesis. The purpose of doing so is to inspect whether there are any clear trends in the energy dependence of the TCSs for these species, that could be somehow traced back to the basic physico-chemical properties of the molecules in question. Hence, throughout this discussion we should keep in mind those values for their most important physico-chemical properties, which are summarized in Table 6.15. When comparing the various TCSs with each other, please also remember that the errors plotted in Fig. 6.19 are the statistical components only of the overall uncertainties on our data and are at the ± 1 standard deviation level. Nevertheless, the overall uncertainties of the measurements on these species have been estimated to be at worst in the 5-15% range (see previous sections).

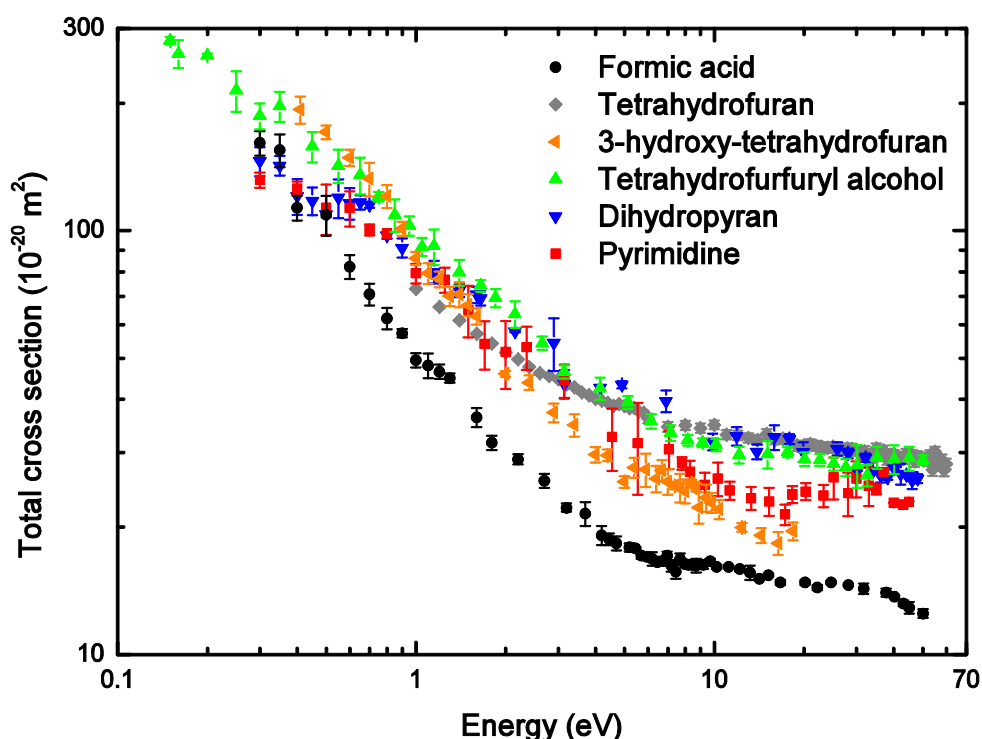


Fig. 6.19. Comparison of the present total cross sections for positron scattering from the molecules of biological interest pertaining to this thesis. See legend in figure for further details.

At a first glance, Fig. 6.19 immediately suggests just how the TCSs for these six biomolecules have a very similar behaviour, as a function of the positron incident energy, although their magnitude in some cases is a little different. Namely the TCSs typically decrease monotonically in magnitude as the incident positron energy increases until first the respective energy

thresholds for positronium formation, then the electronic-excitation states and finally the direct ionisation (see Table 6.15) channel are progressively reached. The opening of these channels has a visible impact on the TCS: it is usually marked by a clear change in the TCS slope or the appearance of a small “bump” in the shape of the TCS, in the proximity or straight after the corresponding energy threshold (see Fig. 6.19). Owing to the opening of all these channels, the TCS at higher energies (at least to the upper limit of energy in our investigations) in quite a few cases seems to essentially be almost a constant function of the energy.

Table 6.15. A selection of the most important physico-chemical properties of the biologically relevant molecules under investigation in the present thesis: formic acid, tetrahydrofuran (THF), 3-hydroxy-tetrahydrofuran (3H-THF), tetrahydrofurfuryl alcohol (THFA), 2,3-dihydropyran (DHP) and pyrimidine. The hard-sphere molecular diameter D , the dipole polarisability α , the permanent dipole moment μ , the first ionisation potential IP and the positronium formation threshold Ps are given for each molecule.

Molecule	D (Å)	α (a.u.)	μ (D)	IP (eV)	Ps (eV)
Formic acid	3.8 ^a	22.5 ^a	1.41 ^b	11.4 ^b	4.6
THF (1 st and 2 nd conformer)	4.63 ^c	47.08	1.96 exp. 1.63 ^d	9.74 ^e	2.94
3H-THF: 1 st conformer 2 nd conformer	> 4.63 ^c	50.68 50.98	1.74 2.88	9.8 ^f	3.0
THFA	> 4.63 ^c	70.18 ^g	~2 ^h	9.43 ⁱ	2.63
DHP	> 2.8	64.92 ^j	1.38 ^k 1.48 ^l	8.6 ^m	1.8
Pyrimidine	5.5 ⁿ	$\alpha_{xx} \sim 69$ ^{o,p} $\alpha_{yy} \sim 71$ ^{o,p} $\alpha_{zz} \sim 38$ ^{o,p} $\bar{\alpha} \sim 59$	2.28-2.39 ^{q-s}	9.33-9.73 ^{t-x}	2.53-2.93

References: ^a Vizcaino *et al.* (2006); ^b Lide (1998); ^c Dampc *et al.* (2007b); ^d Bouchiha *et al.* (2007); ^e Inoue *et al.* (1993); ^f Giardini *et al.* (2005); ^g Szymtkowski and Ptasńska-Denga (2011); ^h Mozejko *et al.* (2006a); ⁱ Milosavljević *et al.* (2010); ^j <http://www.chemspider.com/Chemical-Structure.7789.htm>; ^k Soundararajan and Anantkrishnan (1953); ^l Scanlon *et al.* (1995); ^m Planckaert *et al.* (1974); ⁿ Spears and El-Manguch (1977); ^o Hattig *et al.* (1998); ^p Jansik *et al.* (2004); ^q Blackman *et al.* (1970); ^r Chen and Holroyd (1996); ^s Kisiel *et al.* (1999); ^t Bergmann (1969); ^u Buff and Dannacher (1984); ^v Dewar and Worley (1969); ^w Piancastelli *et al.* (1983); ^x Potts *et al.* (2003).

The origin of the low energy trend in the TCSs for each species, i.e. below the positronium threshold, where only the elastic, rotational and vibrational channels are open, has already been discussed in the previous sections in detail for each particular case. Here, we reiterate that this TCS behaviour is likely to be a general low-energy feature of positron TCSs,

which is thought to be due to the long-range dipole interactions between the respective species and the incident positrons. At these low energies, in fact, the dynamics of the positron scattering process is guided by the competition between the repulsive short-range static interaction, due to the mean field of the positive nucleus of the molecule, and the attractive dipole interaction created by the polarisation of the target molecule induced by the incoming positron (see Chapter 1) and the species permanent dipole moment, not to mention the attractive contribution of virtual positronium. Since the present biomolecular species are all characterised by a large dipole moment and a more or less significant polarisability (see Table 6.15), the negative dipole interaction between the incoming positron and the target molecule typically dominates over the positive static mean field of the target nucleus in this low energy range. Hence, the overall potential driving the collisional interaction becomes largely negative (i.e. attractive) and so the probability of scattering between the projectile and the target is enhanced. This circumstance is well reflected by the increased magnitudes of the TCSs that we observe in Fig. 6.19 at the very low energies (that is below positronium threshold), compared to the higher energies (i.e. above that positronium threshold).

Let us compare now the behaviour between the respective species (Fig. 6.19), to seek for any analogy in the trends of the TCSs that we can tentatively ascribe to the similarity in the physico-chemical properties of those molecules (Table 6.15). Note that this plan is somewhat complicated by the fact that at the lowest energies our measured TCSs are affected by the convolution of the exact TCS over the energy resolution of the positron beam used to investigate the species in question. Also note that the extent of this effect depends on the actual shape of the TCS as a function of the energy, so it is probably a little different for each species. On the other hand, at the higher energies, the several inelastic channels that successively open (positronium, direct ionisation and electronic excitations), are at somewhat different energy values for each species, which also complicates the interpretation of the comparison between these results. By broadening our scope, however, several general trends in the TCSs emerge from Fig. 6.19 and we are now going to discuss them more in detail. We first reiterate that the most immediate and striking aspect of Fig. 6.19 is the remarkable similarity in the qualitative (shape) energy dependence of the TCSs, for each species, in the energy range we have investigated. This resemblance between the various TCSs is seen despite some obvious differences due to the dissimilar thresholds in the opening of the inelastic channels.

First, we try to assess if the dipole polarisability α of these biomolecular species has any effect on the magnitude of their TCSs. To ascertain this we can group the molecules based on the magnitude of their polarisability and see if this subdivision has a parallel equivalent, in Fig. 6.19, to the patterns of the various TCS magnitudes. We can discern the present molecules in the following way:

- Group 1 – species with a “low” polarisability ($\alpha < 30$ a.u.): formic acid;
- Group 2 – species with a “mid” polarisability ($30 \leq \alpha \leq 60$ a.u.): THF, 3H-THF, pyrimidine;

- Group 3 – species with a “high” polarisability ($\alpha > 60$ a.u.): DHP, THFA. We can clearly see in Fig. 6.19 that the absolute magnitudes and shapes of the TCS for the species within each group (i.e. with almost equivalent polarisability) are very similar to each other, to within the total uncertainties on the measurements. For instance, within the second group, the conformers of both THF (Giuliani *et al.*, 2009) and 3H-THF, as well as pyrimidine, have similar values for their dipole polarisability (Table 6.15) and their corresponding TCSs are almost identical, at least below the respective thresholds of the first inelastic process (Fig. 6.19). Above that energy, the inelastic scattering channels seem to increasingly dominate the THF TCS (see Section 6.3 and Fig. 6.9), so that its magnitude becomes larger at higher energies compared to that of 3H-THF and pyrimidine. Another exception to this remark is at the lowest energies where the effect of the convolution over the beam energy width is highest and where 3H-THF seems to display higher TCS values. As noted above, however, this is likely due to the effect of the much larger dipole moment of its second conformer.

In addition, the TCS magnitude between the different groups appears to scale somehow with the respective polarisability range (Fig. 6.19). For example, group 2 shows significantly larger TCSs than that of group 1, which is characterised by a much lower polarisability. Similarly, the group 2 cross sections are also (uniformly) appreciably smaller compared to those of group 3, whose members possess a much bigger polarisability than those of group 2. The TCS of THF (group 2) possibly represents an exception to this correspondence, since its magnitude at the highest energies is as large as that of the molecules of groups 3. As we have already observed above, this is likely to be due to the large contribution of the inelastic channels to the TCS. This polarisability-TCS magnitude correlation makes good physical sense, as the target dipole polarisability in some sense indicates the spatial extent of the molecular orbitals, so that the more extended is this electron cloud distribution the more likely an incident positron will interact with it. The relationship between α and the TCS, that we propose here, is also not a new concept to the ATMOP community, as the San Diego group have previously established a clear empirical connection between the value of the positron binding energy (Danielson *et al.*, 2009) and the value of α for many species (Gribakin *et al.*, 2010). Makochekanwa *et al.* (2009), who reported the positronium formation cross sections for water and formic acid, had also observed a link between those cross sections and the dipole polarisability of the respective species. Therefore, the key role played by the target dipole polarisability on the low energy positron scattering dynamics is well established.

We focus now our attention on the comparison between the present results for THF and 3H-THF, that are related to each other to a high degree, both because of their very similar molecular structure (see Fig. 6.1) and their almost equivalent physico-chemical properties (see Table. 6.15). In Section 6.3 we have already compared the present THF TCS results with those obtained by Zecca *et al.* (2005) (see Fig. 6.8), while in Section 6.4 we have seen how the present 3H-THF data relate with the THF data by Zecca *et al.* (2005) (see Fig. 6.13), so that here we can simply join the two

discussions to draw some conclusions. We, therefore, can say that the present TCSs for THF and 3H-THF are very similar in magnitude below the positronium formation threshold (~ 3 eV) and down to the lowest common energy (1 eV), where they also seem to be consistent with each other, to within the combined overall error bars on the respective data. Yet, in this energy range the TCSs appear to possess two very different energy behaviours: $\sim 1/E$ for 3H-THF and $\sim 1/\sqrt{E}$ for THF. Since the present THF data do not go further down in energy, it is not possible to compare with the 3H-THF data at the lowest energies. However, as particularly shown by Fig. 6.8, at the lowest energies the present THF TCS seems to follow the same trend of the data by Zecca *et al.* (2005), so that below 1 eV it is reasonable to expect it to be tending to the same magnitude and share the same shape. In this case the present 3H-THF TCS would be much larger in magnitude than that of THF, a circumstance that we interpreted in Section 6.4 to be due likely to the effect of the presence in the target sample of the second most stable 3H-THF conformer with its bigger permanent dipole moment, compared to both that of its global minimum conformer and those of THF (see Table 6.15). Above the positronium formation threshold, instead, the interpretation of the present results for THF and 3H-THF is rather complicated by the various inelastic scattering channels becoming open. Therefore we do not discuss this energy range any further, except to note that the 3H-THF TCS is significantly lower in magnitude (by about one third) than that of the parent molecule THF.

The TCS of DHP (see Fig. 6.19) deserves a special comment. While DHP has the second largest dipole polarisability of all the biological species in this study after THFA, its TCS is almost identical to that of the second group in the energy range between ~ 0.5 eV and its positronium formation threshold. We believe this simply reflects the fact that DHP has a permanent dipole moment which is, together with that of formic acid, the smallest among the biomolecules we consider. As a result, the dipole interaction induced by the target polarisability may be compensating for the long-range interaction due to the target permanent dipole moment. Hence, both these long-range interactions are important when looking at the comparative behaviour of these systems.

Finally, let us comment on an intriguing feature of the TCSs that we have observed in all the present measurements. The energy dependence of the positron TCSs at energies below the positronium formation threshold appears to be mainly a monotonic decrease with a slope that equates to either $\sim 1/E$ or $\sim 1/\sqrt{E}$. The $\sim 1/E$ TCS behaviour is seen with the targets formic acid and 3H-THF. On the other hand, THFA, DHP and pyrimidine show a $\sim 1/\sqrt{E}$ dependence. We have also seen these same trends in our measurements on atoms and other molecules (see previous chapters), so that we do not think it can simply be a coincidence. Unfortunately there is no theoretical hint for why these particular trends should be observed and so, in the absence of theoretical guidance, this mystery has been puzzling us for quite some time now. Note, however, that the present total cross sections are uncorrected for the forward angle scattering effect and they are also convoluted over the finite energy resolution of the positron beam. As these

two effects can significantly affect the magnitude of the total cross sections, the energy dependence of the very low energy measured cross sections may vary with respect to what we observed in this thesis.

6.9 Summary and conclusions

We have presented an extensive series of absolute cross section measurements for positron collisions with six molecules of biological relevance: formic acid, tetrahydrofuran, 3-hydroxy-tetrahydrofuran, tetrahydrofurfuryl alcohol, 2,3-dihydropyran and pyrimidine. In all cases the effect of the target molecular dipole moment and dipole polarisability on the dynamics of the scattering process and thus on the TCS behaviour and magnitude was apparent, especially at lower incident positron energies, where the TCSs significantly increase in magnitude towards the low energies. Our interpretation of this typical TCS energy pattern is that these two important molecular properties are strong enough to make the attractive dipole interaction prevail over the repulsive static interaction between the incident positron and the target molecule, so that the probability of scattering is enhanced at low energies. By comparing the data for the different species in an attempt to uncover any underlying trends, we found a strong semi-empirical quantitative correlation between the value of the target dipole polarisability and the TCS magnitude. The permanent dipole moment of the molecule in question was also observed to play an important, although possibly more secondary, role in the scattering dynamics, except perhaps at very low positron impact energies, where there was some evidence for its key relevance in the collision process.

What about the implications of the present TCS results for these biological, important species, on the issue of radiation damage at the molecular level? It is now well known as a result of the research carried out by both the Berlin (Hanel *et al.*, 2003) and Innsbruck (Sulzer *et al.*, 2006) groups, that dissociative electron attachment at near-zero energies can be an important process and have crucial effects on biomolecular systems. So far there has been no observation of an analogous process taking place with positrons. Nevertheless, if it ever turns out that positrons can similarly bind (Danielson *et al.*, 2010), our measured TCSs, with their large magnitude at epithermal energies, might well have important implications in a fundamental understanding of how positrons interact with biological matter and what their effect is. This, however, still represents a speculation at this time. Notwithstanding that point, it is certain that these TCSs are essential for particle track simulation codes, which need realistic atomic and molecular collision data as an input (Sanz *et al.*, 2012).